Received: 5 February 2022 | Revised: 8 April 2022 | Accepted: 11 April 2022

DOI: 10.1002/wcms.1619

FOCUS ARTICLE

WIREs COMPUTATIONAL MOLECULAR SCIENCE WILEY

# New phase space formulations and quantum dynamics approaches

**Xin He** | **Baihua Wu** | **Youhao Shang** | **Bingqi Li** | **Xiangsong Cheng** | **Jian Liu**

Beijing National Laboratory for Molecular Sciences, Institute of Theoretical and Computational Chemistry, College of Chemistry and Molecular Engineering, Peking University, Beijing, China

**Correspondence**
Jian Liu, Beijing National Laboratory for Molecular Sciences, Institute of Theoretical and Computational Chemistry, College of Chemistry and Molecular Engineering, Peking University, Beijing 100871, China.
Email: jianliupku@pku.edu.cn

**Funding information**
Ministry of Science and Technology of the People's Republic of China, Grant/Award Number: 2017YFA0204901; National Natural Science Foundation of China, Grant/Award Number: 21961142017

**Edited by:** Jinlong Yang, Associate Editor and Peter R. Schreiner, Editor-in-Chief

**Abstract**

We report recent progress on the phase space formulation of quantum mechanics with coordinate-momentum variables, focusing more on new theory of (weighted) constraint coordinate-momentum phase space for discrete-variable quantum systems. This leads to a general coordinate-momentum phase space formulation of composite quantum systems, where conventional representations on infinite phase space are employed for continuous variables. It is convenient to utilize (weighted) constraint coordinate-momentum phase space for representing the quantum state and describing nonclassical features. Various numerical tests demonstrate that new trajectory-based quantum dynamics approaches derived from the (weighted) constraint phase space representation are useful and practical for describing dynamical processes of composite quantum systems in the gas phase as well as in the condensed phase.

This article is categorized under:

Molecular and Statistical Mechanics > Molecular Dynamics and Monte-Carlo Methods

Theoretical and Physical Chemistry > Reaction Dynamics and Kinetics

Theoretical and Physical Chemistry > Statistical Mechanics

**KEYWORDS**

composite quantum systems, constraint phase space, nonadiabatic dynamics, phase space formulation, quantum dynamics

## 1 | INTRODUCTION

Phase space with coordinate-momentum variables is a fundamental concept and offers a convenient tool to describe statistics as well as dynamics in classical mechanics. In comparison to other equivalent interpretations of quantum mechanics, phase space formulations offer more insight and understanding between quantum and classical counterpart concepts, which are widely used in chemical and biological dynamics and spectroscopy,[1–60] quantum optics,[51,61–70] cryogenic physics/chemistry,[71–75] quantum information and computation,[76–87] and so forth.

Phase space formulations of quantum mechanics have been developed since two important pioneering works, the Weyl transform in 1927, of which the original formulation converted a Hamiltonian on classical phase space into a quantum mechanical operator,[88] and the Wigner function in 1932 that in principle depicts the inverse transform although a pure state was used for demonstration.[89] The most essential element is the one-to-one correspondence

  

mapping between quantum operators and classical functions often defined on a smooth manifold, namely, phase space. Because of the commutation relation of conjugate operators, the mapping is not unique in quantum mechanics.[90,91]

When infinite phase space is employed for a continuous-variable quantum system, most phase space formulations can be described by Cohen's generalized form[92] in 1966. Quantum dynamics with phase space variables is expressed by the Moyal or Moyal-like bracket as first proposed by Groenewold[93] in 1946 and Moyal[94] in 1949. The Wigner and Husimi representations are most often used for the continuous-variable system. When the Moyal bracket is approximated by the Poisson bracket in the Wigner phase space expression of the quantum Liouville theorem, which was also derived as the linearized semiclassical initial value representation (LSC-IVR) or classical Wigner model[4–8,11,20,23] for the quantum correlation function, it reproduces exact quantum correlation functions even of nonlinear operators (i.e., nonlinear functions of the coordinate or momentum operator) in the harmonic or classical limit. The truncated Wigner approximation[74] with the time-dependent generalization of the Bopp representation[90,95] is similar to the LSC-IVR, but the former requests more demanding evaluation of the stability matrix elements along the trajectory when nonlinear operators are involved in the correlation function. Liu and Miller[15] suggest a practical way to implement the imaginary time path integral treatment of the Boltzmann density operator in the LSC-IVR for general molecular systems that often contain imaginary frequencies. Its recent application illustrates that quantum dynamical effects play a critical role in reproducing the peaks in the intermediate region between the librational and bending bands, those between the bending and stretching bands, and the double-peak in the stretching band in the experimental isotropic Raman spectrum of liquid water[19] (as shown in Figure 1). In addition that more advanced versions of SC-IVR[96–99] are capable of improving over the LSC-IVR, in Reference 11, we first employed the quantum Liouville theorem in the phase space formulation to develop trajectory-based approaches to satisfy the two fundamental criteria: conservation of the quantum Boltzmann distribution for the thermal equilibrium system and being exact for any quantum thermal correlation functions in the classical and harmonic limits. Such trajectory-based approaches can in principle be further improved by higher order corrections of the exact series expansion of the phase space propagator as demonstrated in Reference 44. More progress along this line can be found in References 37–47. (Figure 2 shows molecular vibrational spectra produced by the new phase space quantum dynamics methods.)

Phase space representations of a finite discrete $F$-state quantum system were first independently described by Stratonovich[100] in 1956, Feynman[101] in 1987, and Wootters[102] in 1987. Further developments of Stratonovich's formulation have focused on an SU(2) or SU($F$) structure of phase space,[103–117] while those on the construction of a discrete phase space are described in References 78,118–126. Other than the 2-state (or spin 1/2) system, the exact equations of motion

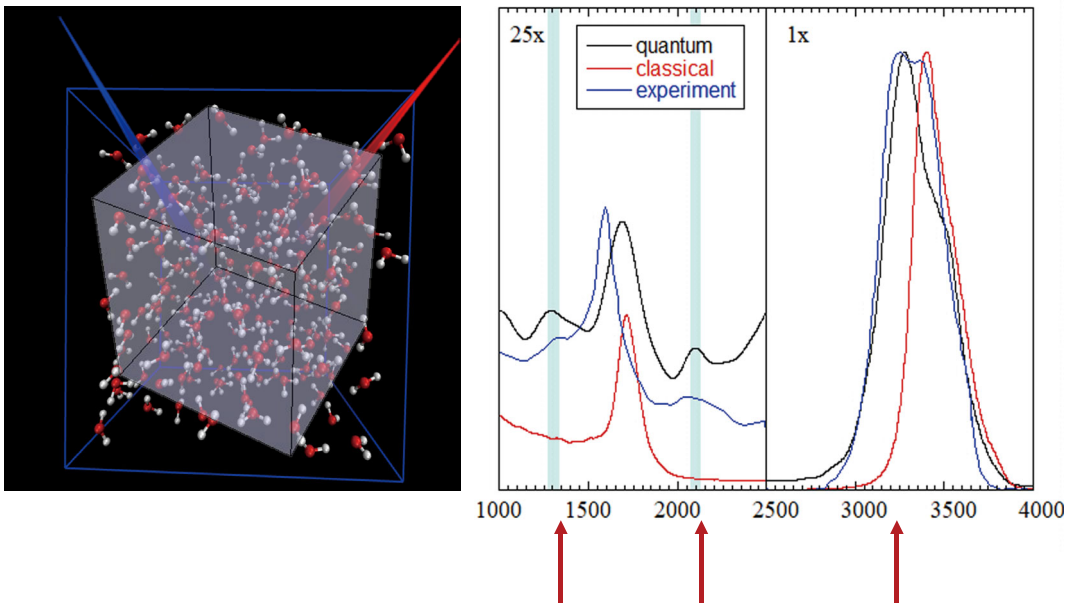


FIGURE 1 Quantum dynamical effects are decisive in reproducing the experimental isotropic Raman spectrum of liquid water at room temperature, as illustrated by the LSC-IVR simulation where infinite (Wigner) phase space for nuclear DOFs is used. Converged results were obtained with 216 water molecules in a box with periodic boundary conditions. (Reprinted with permission from Reference 19, Copyright 2018, Taylor & Francis).

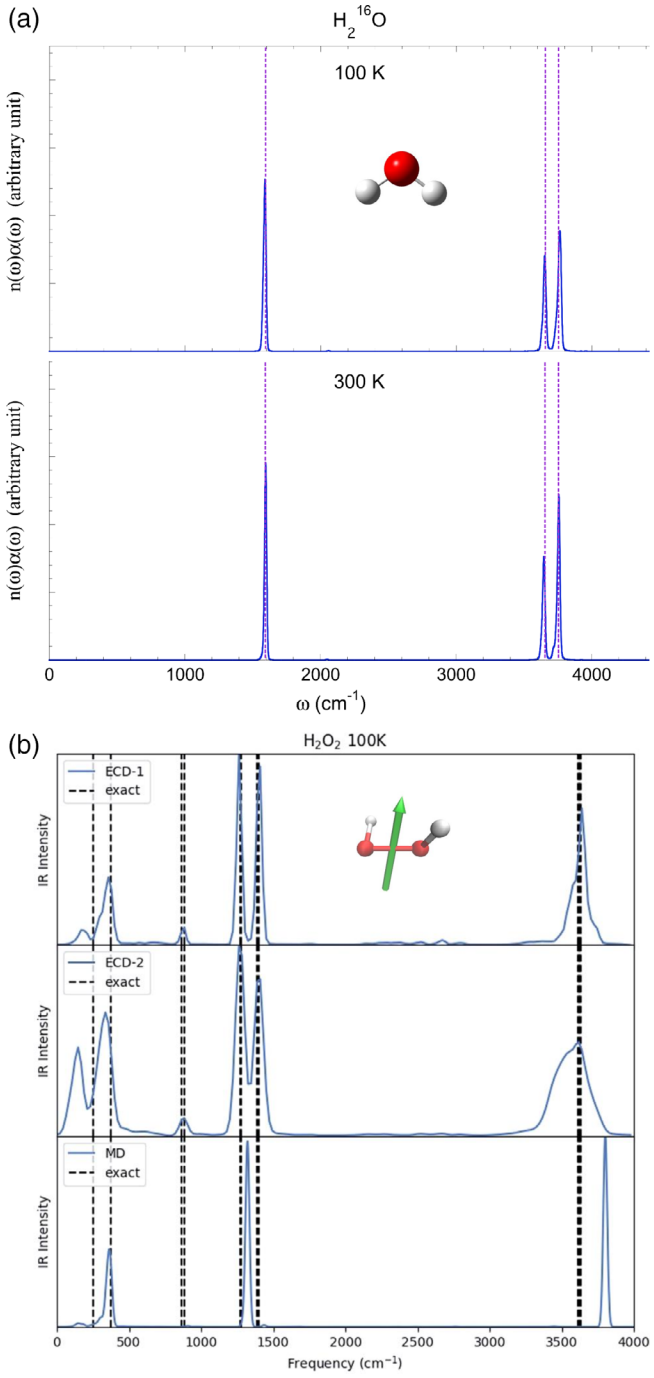


**FIGURE 2** Molecular vibrational spectra produced by more advanced trajectory-based dynamics methods with infinite (Wigner) phase space used for nuclear DOFs, which satisfy the two fundamental criteria: Conservation of the quantum Boltzmann distribution for the thermal equilibrium system and being exact for any quantum thermal correlation functions in the classical and harmonic limits. (a) Vibrational spectrum of the $H_2O$ molecule at 100 K and that at 300 K. Reprinted with permission from Reference 41, Copyright 2016 American Institute of Physics publishing. (b) Vibrational spectrum of the $H_2O_2$ molecule at 100 K. Reprinted with permission from Reference 44, Copyright 2021, American Institute of Physics publishing.

(EOMs) of phase variables (expressed by the Moyal-like bracket) involved in these approaches for the finite discrete multi-state system are often tedious and numerically unfavourable.[109,127–130,299,302] (See Appendix 3 of the Supporting Information for more discussion.) Recent theoretical progress on exactly mapping the finite discrete $F$-state quantum system onto *constraint* coordinate-momentum phase space suggests that there exists a novel unified framework to derive comprehensive exact mapping Hamiltonians,[44,57,131,132] of which the quantum EOMs of mapping coordinate-momentum variables are simply linear.[44,57,131–134]

The unified mapping formulation on coordinate-momentum phase space[44,57,131–134] then offers a useful tool to treat dynamics of a composite quantum system, in which both continuous and finite discrete degrees of freedom (DOFs) are involved and coupled with one another. Because a typical molecular system has vibrational, rotational, and translational motion, it is often much more convenient to employ continuous coordinate space rather than Hilbert space with dense states to describe the nuclear DOFs. On the other hand, the energy gap between different electronic states of interest is often significantly larger such that the (adiabatic or diabatic) state representation is more useful to depict the electronic DOFs. It is evident that a general description of the molecular system leads to a composite quantum system, especially in the nonadiabatic region.[135–152] A comprehensive version of the Meyer–Miller mapping Hamiltonian model[153,154] can rigorously be formulated in the general coordinate-momentum phase space formulation.[44,57,131–134]

In the Focus Article, we focus on novel developments on the phase space formulation of quantum mechanics with coordinate-momentum variables for discrete-variable systems as well as for composite systems.[44,57,131–134] In Section 2, we first review the general coordinate-momentum phase space formulation, where infinite space is used for describing continuous variables and constraint space is employed for mapping discrete variables. We then propose a weighted constraint phase space representation that is also an exact formulation for mapping discrete-variable quantum systems. Section 3 demonstrates several examples and discusses implications of the (weighted) constraint coordinate-momentum phase space for studying and illustrating discrete-variable or composite quantum systems. When we use the weighted constraint phase space representation for mapping composite quantum systems, the mapping Hamiltonian (we use the Meyer–Miller mapping Hamiltonian for demonstration throughout the article, albeit that other mapping Hamiltonians are also available[57,58,131,132]) yields a novel trajectory-based approximate approach for composite systems. Such a new method satisfies the frozen nuclei limit [i.e., the dynamics reproduces the exact evolution when only finite discrete (electronic) DOFs are involved]. In Section 4, the performance of new trajectory-based quantum dynamics approaches on (weighted) constraint phase space is extensively tested for a few typical benchmark composite systems in the gas phase as well as in the condensed phase. Finally, conclusion remarks are presented in Section 5.

## 2 | GENERAL COORDINATE-MOMENTUM PHASE SPACE FORMULATION OF QUANTUM MECHANICS

Consider a (molecular) system with $N$ continuous (nuclear) DOFs and $F$ discrete (electronic) states, of which the Hamiltonian reads

$$\widehat{H} = \sum_{n,m=1}^{F} H_{nm}\left(\widehat{\mathbf{R}},\widehat{\mathbf{P}}\right)|n\rangle\langle m| = \sum_{n,m=1}^{F}\left[\frac{1}{2}\widehat{\mathbf{P}}^{\mathrm{T}}\mathbf{M}^{-1}\widehat{\mathbf{P}}\delta_{nm} + V_{nm}\left(\widehat{\mathbf{R}}\right)\right]|n\rangle\langle m|, \tag{1}$$

where $\mathbf{R}$ and $\mathbf{P}$ are the nuclear coordinate and momentum variables, respectively, $\mathbf{M}$ is the diagonal mass matrix, and the $F$ states form an orthonormal complete basis set, that is,

$$< m|n > = \delta_{mn}, \widehat{I}_{\mathrm{ele}} = \sum_{n=1}^{F}|n\rangle\langle n|. \tag{2}$$

$\widehat{I}_{\mathrm{ele}}$ and $\widehat{I}_{\mathrm{nuc}}$ stand for the identity operator of the discrete (electronic) DOFs and that of the continuous (nuclear) DOFs. For simplicity, Equation (1) employs the (electronically) diabatic representation, where the Hermitian potential matrix $\mathbf{V}(\mathbf{R})$ is a function of only the coordinate vector. (In applications $\mathbf{V}(\mathbf{R})$ is often a real symmetric matrix.) More discussion on the adiabatic representation of discrete (electronic) DOFs is available in Section 4.1.

The unified formulation of mapping phase space with coordinate-momentum variables offers a useful exact approach to describe the composite system. The trace of a product of two quantum operators is expressed as an integral of two functions on mapping phase space, that is,

$$\mathrm{Tr}_{n,e}\left[\widehat{A}\widehat{B}\right] = \int \mathrm{d}\boldsymbol{\mu}_{\mathrm{nuc}}(\mathbf{R},\mathbf{P})\int_{\mathcal{S}(\mathbf{x},\mathbf{p})}\mathrm{d}\boldsymbol{\mu}_{\mathrm{ele}}(\mathbf{x},\mathbf{p})A_C(\mathbf{R},\mathbf{P};\mathbf{x},\mathbf{p})\widetilde{B}_C(\mathbf{R},\mathbf{P};\mathbf{x},\mathbf{p}) \tag{3}$$

with

$$A_C(\mathbf{R},\mathbf{P};\mathbf{x},\mathbf{p}) = \mathrm{Tr}_{n,e}\left[\widehat{A}\widehat{K}_{\mathrm{nuc}}(\mathbf{R},\mathbf{P})\bigotimes\widehat{K}_{\mathrm{ele}}(\mathbf{x},\mathbf{p})\right], \tag{4}$$

$$\widetilde{B}_C(\mathbf{R},\mathbf{P};\mathbf{x},\mathbf{p}) = \mathrm{Tr}_{n,e}\left[\widehat{K}^{-1}_{\mathrm{nuc}}(\mathbf{R},\mathbf{P})\bigotimes\widehat{K}^{-1}_{\mathrm{ele}}(\mathbf{x},\mathbf{p})\widehat{B}\right], \tag{5}$$

$\mathrm{d}\boldsymbol{\mu}_{\mathrm{nuc}}(\mathbf{R},\mathbf{P}) = (2\pi\hbar)^{-N}\mathrm{d}\mathbf{R}\mathrm{d}\mathbf{P}$ and $\mathrm{d}\boldsymbol{\mu}_{\mathrm{ele}}(\mathbf{x},\mathbf{p}) = F\mathrm{d}\mathbf{x}\mathrm{d}\mathbf{p}$ as the integration measure on nuclear phase space and that on electronic phase space, respectively, and $\mathrm{Tr}_{n,e}$ represents the trace over the corresponding nuclear and electronic Hilbert space. The integral over the mapping phase space variables for the finite discrete (electronic) DOFs in Equation (3) is performed as

$$\int_{\mathcal{S}(\mathbf{x},\mathbf{p})} F\mathrm{d}\mathbf{x}\mathrm{d}\mathbf{p}g(\mathbf{x},\mathbf{p}) = \int F\mathrm{d}\mathbf{x}\mathrm{d}\mathbf{p}\frac{1}{\Omega}\mathcal{S}(\mathbf{x},\mathbf{p})g(\mathbf{x},\mathbf{p}) = \int F\mathrm{d}\mathbf{x}\mathrm{d}\mathbf{p}\overline{\mathcal{S}}(\mathbf{x},\mathbf{p})g(\mathbf{x},\mathbf{p}), \tag{6}$$

where the area of constraint space $\mathcal{S}(\mathbf{x},\mathbf{p})$

$$\Omega = \int \mathrm{d}\mathbf{x}\mathrm{d}\mathbf{p}\mathcal{S}(\mathbf{x},\mathbf{p}) \tag{7}$$

is the normalization constant, and $\overline{\mathcal{S}}(\mathbf{x},\mathbf{p})$ is the normalized constraint space.

The normalization of the (inverse) mapping kernel reads

$$\mathrm{Tr}_n\left[\widehat{K}_{\mathrm{nuc}}(\mathbf{R},\mathbf{P})\right] = \mathrm{Tr}_n\left[\widehat{K}^{-1}_{\mathrm{nuc}}(\mathbf{R},\mathbf{P})\right] = 1 \tag{8}$$

$$\mathrm{Tr}_e\left[\widehat{K}_{\mathrm{ele}}(\mathbf{x},\mathbf{p})\right] = \mathrm{Tr}_e\left[\widehat{K}^{-1}_{\mathrm{ele}}(\mathbf{x},\mathbf{p})\right] = 1 \tag{9}$$

and

$$\int \mathrm{d}\boldsymbol{\mu}_{\mathrm{nuc}}(\mathbf{R},\mathbf{P})\ \widehat{K}_{\mathrm{nuc}}(\mathbf{R},\mathbf{P}) = \int \mathrm{d}\boldsymbol{\mu}_{\mathrm{nuc}}(\mathbf{R},\mathbf{P})\ \widehat{K}^{-1}_{\mathrm{nuc}}(\mathbf{R},\mathbf{P}) = \widehat{I}_{\mathrm{nuc}} \tag{10}$$

$$\int_{\mathcal{S}(\mathbf{x},\mathbf{p})} \mathrm{d}\boldsymbol{\mu}_{\mathrm{ele}}(\mathbf{x},\mathbf{p})\widehat{K}_{\mathrm{ele}}(\mathbf{x},\mathbf{p}) = \int_{\mathcal{S}(\mathbf{x},\mathbf{p})} \mathrm{d}\boldsymbol{\mu}_{\mathrm{ele}}(\mathbf{x},\mathbf{p})\widehat{K}^{-1}_{\mathrm{ele}}(\mathbf{x},\mathbf{p}) = \widehat{I}_{\mathrm{ele}}. \tag{11}$$

The one-to-one correspondence mapping from phase space function $A_C(\mathbf{R},\mathbf{P};\mathbf{x},\mathbf{p})$ or $\widetilde{B}_C(\mathbf{R},\mathbf{P};\mathbf{x},\mathbf{p})$ of Equation (4) back to operator $\widehat{A}$ or $\widehat{B}$ is

$$\begin{aligned}
\widehat{A} &= \int \mathrm{d}\boldsymbol{\mu}_{\mathrm{nuc}}(\mathbf{R},\mathbf{P})\int_{\mathcal{S}(\mathbf{x},\mathbf{p})} \mathrm{d}\boldsymbol{\mu}_{\mathrm{ele}}(\mathbf{x},\mathbf{p})A_C(\mathbf{R},\mathbf{P};\mathbf{x},\mathbf{p})\widehat{K}^{-1}_{\mathrm{nuc}}(\mathbf{R},\mathbf{P})\bigotimes\widehat{K}^{-1}_{\mathrm{ele}}(\mathbf{x},\mathbf{p}) \\
\widehat{B} &= \int \mathrm{d}\boldsymbol{\mu}_{\mathrm{nuc}}(\mathbf{R},\mathbf{P})\int_{\mathcal{S}(\mathbf{x},\mathbf{p})} \mathrm{d}\boldsymbol{\mu}_{\mathrm{ele}}(\mathbf{x},\mathbf{p})\widetilde{B}_C(\mathbf{R},\mathbf{P};\mathbf{x},\mathbf{p})\widehat{K}_{\mathrm{nuc}}(\mathbf{R},\mathbf{P})\bigotimes\widehat{K}_{\mathrm{ele}}(\mathbf{x},\mathbf{p}).
\end{aligned} \tag{12}$$

The nuclear or electronic kernel should satisfy five criteria, namely, linearity, reality, standardization (normalization), traciality, and covariance.[93,94,100,115]

## 2.1 | Mapping kernel for continuous (nuclear) degrees of freedom

The integrals for $(\mathbf{R},\mathbf{P})$ in Equations (3), (10), and (12) are over infinite (nuclear) phase space. The mapping kernel and its inverse for the nuclear DOFs are

$$\begin{aligned}\widehat{K}_{\rm nuc}(\mathbf{R},\mathbf{P}) &= \left(\frac{\hbar}{2\pi}\right)^N \int d\boldsymbol{\zeta} \int d\boldsymbol{\eta} e^{i\boldsymbol{\zeta}\cdot\left(\widehat{\mathbf{R}}-\mathbf{R}\right)+i\boldsymbol{\eta}\cdot\left(\widehat{\mathbf{P}}-\mathbf{P}\right)} f(\boldsymbol{\zeta},\boldsymbol{\eta}) \\ \widehat{K}^{-1}_{\rm nuc}(\mathbf{R},\mathbf{P}) &= \left(\frac{\hbar}{2\pi}\right)^N \int d\boldsymbol{\zeta} \int d\boldsymbol{\eta} e^{i\boldsymbol{\zeta}\cdot\left(\widehat{\mathbf{R}}-\mathbf{R}\right)+i\boldsymbol{\eta}\cdot\left(\widehat{\mathbf{P}}-\mathbf{P}\right)} [f(-\boldsymbol{\zeta},-\boldsymbol{\eta})]^{-1},\end{aligned} \tag{13}$$

where $f(\boldsymbol{\zeta},\boldsymbol{\eta})$ is a scalar function. For example, we have the Wigner function[89,155]

$$f(\boldsymbol{\zeta},\boldsymbol{\eta}) = 1, \tag{14}$$

the Husimi function[156]

$$f(\boldsymbol{\zeta},\boldsymbol{\eta}) = \exp\left(-\frac{\boldsymbol{\zeta}^T\boldsymbol{\Gamma}^{-1}\boldsymbol{\zeta}}{4} - \frac{\hbar^2}{4}\boldsymbol{\eta}^T\boldsymbol{\Gamma}\boldsymbol{\eta}\right), \tag{15}$$

the anti-Husimi function

$$f(\boldsymbol{\zeta},\boldsymbol{\eta}) = \exp\left(\frac{\boldsymbol{\zeta}^T\boldsymbol{\Gamma}^{-1}\boldsymbol{\zeta}}{4} + \frac{\hbar^2}{4}\boldsymbol{\eta}^T\boldsymbol{\Gamma}\boldsymbol{\eta}\right), \tag{16}$$

the Glauber–Sudarshan P function[61,62,66] (with the characteristic frequency matrix $\boldsymbol{\omega}$ of the system)

$$f(\boldsymbol{\zeta},\boldsymbol{\eta}) = \exp\left[\frac{\hbar}{4}\boldsymbol{\zeta}^T\mathbf{M}^{-1/2}\boldsymbol{\omega}^{-1}\mathbf{M}^{-1/2}\boldsymbol{\zeta} + \frac{\hbar}{4}\boldsymbol{\eta}^T\mathbf{M}^{1/2}\boldsymbol{\omega}\mathbf{M}^{1/2}\boldsymbol{\eta}\right], \tag{17}$$

and its generalized versions,[66] the Glauber Q function[157]

$$f(\boldsymbol{\zeta},\boldsymbol{\eta}) = \exp\left[-\frac{\hbar}{4}\boldsymbol{\zeta}^T\mathbf{M}^{-1/2}\boldsymbol{\omega}^{-1}\mathbf{M}^{-1/2}\boldsymbol{\zeta} - \frac{\hbar}{4}\boldsymbol{\eta}^T\mathbf{M}^{1/2}\boldsymbol{\omega}\mathbf{M}^{1/2}\boldsymbol{\eta}\right], \tag{18}$$

the normal–antinormal ordered function[91]

$$f(\boldsymbol{\zeta},\boldsymbol{\eta}) = \cosh\left[\frac{\hbar}{4}\boldsymbol{\zeta}^T\mathbf{M}^{-1/2}\boldsymbol{\omega}^{-1}\mathbf{M}^{-1/2}\boldsymbol{\zeta} + \frac{\hbar}{4}\boldsymbol{\eta}^T\mathbf{M}^{1/2}\boldsymbol{\omega}\mathbf{M}^{1/2}\boldsymbol{\eta}\right], \tag{19}$$

the Kirkwood antistandard-ordered function[158,159]

$$f(\boldsymbol{\zeta},\boldsymbol{\eta}) = e^{i\hbar\boldsymbol{\zeta}^T\boldsymbol{\eta}/2}, \tag{20}$$

the Mehta standard-ordered function[160]

$$f(\boldsymbol{\zeta},\boldsymbol{\eta}) = e^{-i\hbar\boldsymbol{\zeta}^T\boldsymbol{\eta}/2}, \tag{21}$$

the Rivier function[161,162]

$$f(\boldsymbol{\zeta},\boldsymbol{\eta}) = \cos\left[\frac{1}{2}\hbar\boldsymbol{\zeta}^T\boldsymbol{\eta}\right], \tag{22}$$

and the distribution function of Born and Jordan[163]

$$f(\boldsymbol{\zeta},\boldsymbol{\eta}) = \frac{\sin\left[\frac{1}{2}\hbar\boldsymbol{\zeta}^T\boldsymbol{\eta}\right]}{\frac{1}{2}\hbar\boldsymbol{\zeta}^T\boldsymbol{\eta}}, \tag{23}$$

and so forth.

When operator $\widehat{A}$ is a function of only the nuclear DOFs, its phase space function from Equation (4) and the dual function from Equation (5) become

$$A_{\text{nuc}}(\mathbf{R},\mathbf{P}) = \text{Tr}_n\left[\widehat{A}\widehat{K}_{\text{nuc}}(\mathbf{R},\mathbf{P})\right] \tag{24}$$

and

$$\widetilde{A}_{\text{nuc}}(\mathbf{R},\mathbf{P}) = \text{Tr}_n\left[\widehat{K}^{-1}_{\text{nuc}}(\mathbf{R},\mathbf{P})\widehat{A}\right]. \tag{25}$$

When the Wigner function Equation (14) is used, the mapping kernel and its inverse are the same, that is, $\widehat{K}_{\text{nuc}}(\mathbf{x},\mathbf{p}) = \widehat{K}^{-1}_{\text{nuc}}(\mathbf{x},\mathbf{p})$. The Wigner phase space function of operator $\widehat{A}$ (from Equation (24)) is identical to its dual (from Equation (25)),

$$A^W_{\text{nuc}}(\mathbf{R},\mathbf{P}) = \widetilde{A}^W_{\text{nuc}}(\mathbf{R},\mathbf{P}). \tag{26}$$

When the Husimi phase space (Equation (15)) is employed, it is straightforward to show the relationship between the Wigner and Husimi phase space functions (obtained from Equation (24))

$$A^H_{\text{nuc}}(\mathbf{R},\mathbf{P}) = \exp\left[\frac{1}{4}\left(\frac{\text{d}}{\text{d}\mathbf{R}}\right)^T\boldsymbol{\Gamma}^{-1}\left(\frac{\text{d}}{\text{d}\mathbf{R}}\right) + \frac{\hbar^2}{4}\left(\frac{\text{d}}{\text{d}\mathbf{P}}\right)^T\boldsymbol{\Gamma}\left(\frac{\text{d}}{\text{d}\mathbf{P}}\right)\right]A^W_{\text{nuc}}(\mathbf{R},\mathbf{P}), \tag{27}$$

and the relationship between the dual function of Husimi phase space $\widetilde{A}^H_{\text{nuc}}(\mathbf{R},\mathbf{P})$ and the Wigner phase space function $A^W_{\text{nuc}}(\mathbf{R},\mathbf{P})$

$$\widetilde{A}^H_{\text{nuc}}(\mathbf{R},\mathbf{P}) = \exp\left[-\frac{1}{4}\left(\frac{\text{d}}{\text{d}\mathbf{R}}\right)^T\boldsymbol{\Gamma}^{-1}\left(\frac{\text{d}}{\text{d}\mathbf{R}}\right) - \frac{\hbar^2}{4}\left(\frac{\text{d}}{\text{d}\mathbf{P}}\right)^T\boldsymbol{\Gamma}\left(\frac{\text{d}}{\text{d}\mathbf{P}}\right)\right]A^W_{\text{nuc}}(\mathbf{R},\mathbf{P}). \tag{28}$$

Because any choice of $f(\boldsymbol{\zeta},\boldsymbol{\eta})$ in Equation (13) leads to an informationally complete representation of the continuous-variable quantum system, it is not difficult to establish the relationship between different (dual) phase space functions in addition to Equations (27) and (28).

## 2.2 | Mapping kernel on constraint space for discrete (electronic) degrees of freedom

As derived first in appendix A of Reference 132 in the spirit of Reference 131 and then in the Supporting Information of Reference 134, the kernel that maps a set of $F$ states onto constraint phase space $\mathcal{S}(\mathbf{x},\mathbf{p})$ reads

$$\widehat{K}_{\rm ele}(\mathbf{x},\mathbf{p}) = \sum_{n,m=1}^{F} \left[\frac{1}{2}\left(x^{(n)} + ip^{(n)}\right)\left(x^{(m)} - ip^{(m)}\right) - \gamma\delta_{nm}\right] |n\rangle\langle m|, \tag{29}$$

and the corresponding inverse kernel is

$$\widehat{K}^{-1}_{\rm ele}(\mathbf{x},\mathbf{p}) = \sum_{n,m=1}^{F} \left[\frac{1+F}{2(1+F\gamma)^2}\left(x^{(n)} + ip^{(n)}\right)\left(x^{(m)} - ip^{(m)}\right) - \frac{1-\gamma}{1+F\gamma}\delta_{nm}\right] |n\rangle\langle m|. \tag{30}$$

As naturally required by Equation (9), constraint phase space $\mathcal{S}(\mathbf{x},\mathbf{p})$ is defined by

$$\delta\left(\sum_{n=1}^{F}\frac{\left(x^{(n)}\right)^2 + \left(p^{(n)}\right)^2}{2} - (1+F\gamma)\right), \tag{31}$$

of which the area is

$$\Omega(\gamma) = \int \mathrm{d}\mathbf{x}\mathrm{d}\mathbf{p}\,\delta\left(\sum_{n=1}^{F}\frac{\left(x^{(n)}\right)^2 + \left(p^{(n)}\right)^2}{2} - (1+F\gamma)\right). \tag{32}$$

The normalized constraint phase space is $\overline{\mathcal{S}}(\mathbf{x},\mathbf{p}) = \mathcal{S}(\mathbf{x},\mathbf{p})/\Omega(\gamma)$.

Equations (29)–(32) define the mapping kernel and inverse kernel as well as constraint phase space, which are the key elements of the coordinate-momentum phase space formulation of the discrete-variable quantum system that we first established in References 131,132 and further developed in References 57,58,134. As yielded from Equation (4), when the Wigner function Equation (14) is used for the nuclear DOFs, the mapping Hamiltonian for the quantum Hamiltonian operator Equation (1) reads

$$H_C(\mathbf{R},\mathbf{P};\mathbf{x},\mathbf{p};\gamma) = \frac{1}{2}\mathbf{P}^T\mathbf{M}^{-1}\mathbf{P} + \sum_{n,m=1}^{F} V_{mn}(\mathbf{R})\left[\frac{1}{2}\left(x^{(n)} + ip^{(n)}\right)\left(x^{(m)} - ip^{(m)}\right) - \gamma\delta_{nm}\right]. \tag{33}$$

Because $\mathbf{V}(\mathbf{R})$ is Hermitian, the mapping Hamiltonian is real. As $\mathbf{V}(\mathbf{R})$ is often a real symmetric matrix, Equation (33) becomes

$$H_C(\mathbf{R},\mathbf{P};\mathbf{x},\mathbf{p};\gamma) = \frac{1}{2}\mathbf{P}^T\mathbf{M}^{-1}\mathbf{P} + \sum_{n,m=1}^{F}\left[\frac{1}{2}\left(x^{(n)}x^{(m)} + p^{(n)}p^{(m)}\right) - \gamma\delta_{nm}\right]V_{mn}(\mathbf{R}), \tag{34}$$

which is the seminal Meyer–Miller Hamiltonian[153] that has extensively been implemented for nonadiabatic dynamics in the literature.[4,56,60,138,154,164–218] In References 58,131,132, it is shown that there also exist other comprehensive mapping Hamiltonian models in the general coordinate-momentum phase space formulation of quantum mechanics. When the mapping Hamiltonian is employed to generate trajectory-based dynamics in the phase space formulation for a composite quantum system, we denote it as the classical mapping model (CMM) approach. It satisfies the frozen nuclei limit. We use the Meyer–Miller Hamiltonian for demonstration throughout the Focus Article.

When Meyer and Miller proposed the conventional Meyer–Miller mapping Hamiltonian model for the nonadiabatic system in 1979, they did not invoke the phase space formulation. In 1997, Stock and Thoss[154] utilized the Schwinger oscillator theory of angular momentum[219,220] to derive the Meyer–Miller mapping Hamiltonian.[153] Its LSC-IVR approximation[4] in principle includes *infinite* Wigner phase space for the finite set of (electronic) states. The applications, however, suggest that the LSC-IVR approximation in the framework of References 4,154,170 is not good.[172,177,181,187,195,200,202] More advanced semiclassical approaches[96,97] improve the performance but request more

computational effort.[172,173] The symmetric-window function and other techniques have been introduced to practically overcome the drawbacks.[177,181,187,195,200,202] Recent progress along this line is briefly summarized in Reference 138.

Equation (31) indicates that parameter $\gamma$ lies in region $(-1/F,\infty)$. It is shown that parameter $\gamma$ can be either positive or negative[131,134] and should be interpreted as a special case of the commutator matrix[57,58,131,134] rather than the conventional zero-point-energy parameter.[153,154] There exist three key elements for a trajectory-based quantum dynamics method to evaluate the evolution of the expectation/ensemble average of physical property, namely,

1. the EOMs of the trajectory,
2. the initial condition of the trajectory, and
3. the integral expression for the expectation/ensemble average of the physical property of interest.

In the frozen-nuclei limit, Hamilton's EOMs governed by the Meyer–Miller mapping Hamiltonian is isomorphic to exact dynamics. While it is reasonable to employ the mapping Hamiltonian to define the EOMs of the trajectory, the left two elements are also important to consider such that the trajectory-based dynamics method is consistent. The constraint coordinate-momentum phase space formulation then offers a more advanced platform to consider all the three key elements.

It is evident that Equation (31) is a special choice of constraint phase space $\mathcal{S}(\mathbf{x},\mathbf{p})$. The interpretation of parameter $\gamma$ in References 57,58,131,134 hints that a more comprehensive choice of normalized constraint phase space $\overline{\mathcal{S}}(\mathbf{x},\mathbf{p})$ is

$$\int_{-1/F}^{\infty} \mathrm{d}\gamma w(\gamma)\frac{1}{\Omega(\gamma)}\delta\left(\sum_{n=1}^{F}\frac{\left(x^{(n)}\right)^2+\left(p^{(n)}\right)^2}{2}-(1+F\gamma)\right), \tag{35}$$

with the *quasi*-probability distribution function

$$\int_{-1/F}^{\infty} \mathrm{d}\gamma w(\gamma)=1. \tag{36}$$

Equation (6), the integral over the mapping phase space variables for the finite discrete (electronic) DOFs then becomes

$$\begin{aligned}&\int_{\mathcal{S}(\mathbf{x},\mathbf{p})} F\mathrm{d}\mathbf{x}\mathrm{d}\mathbf{p}g(\mathbf{x},\mathbf{p})\\ &=\int_{-1/F}^{\infty}\mathrm{d}\gamma w(\gamma)\int F\mathrm{d}\mathbf{x}\mathrm{d}\mathbf{p}\frac{1}{\Omega(\gamma)}\delta\left(\sum_{n=1}^{F}\frac{\left(x^{(n)}\right)^2+\left(p^{(n)}\right)^2}{2}-(1+F\gamma)\right)g(\mathbf{x},\mathbf{p}).\end{aligned} \tag{37}$$

If we require that the kernel is the same as its inverse, that is,

$$\widehat{K}_{\mathrm{ele}}(\mathbf{x},\mathbf{p})=\widehat{K}_{\mathrm{ele}}^{-1}(\mathbf{x},\mathbf{p})=\sum_{n,m=1}^{F}\left[\frac{1}{2}\left(x^{(n)}+ip^{(n)}\right)\left(x^{(m)}-ip^{(m)}\right)-\gamma\delta_{nm}\right]|n\rangle\langle m|, \tag{38}$$

it is then not difficult to obtain

$$\int_{-1/F}^{\infty}\mathrm{d}\gamma w(\gamma)\chi(\gamma)=1 \tag{39}$$

with

$$\chi(\gamma) = F\gamma^2 + 2\gamma. \tag{40}$$

(See Appendix 1 of the Supporting Information for more discussion.) Equations (35)–(40) define normalized constraint phase space $\overline{\mathcal{S}}(\mathbf{x},\mathbf{p})$, the mapping kernel and inverse kernel, and the *quasi*-probability distribution function $w(\gamma)$ of parameter $\gamma$. The weighted constraint phase space formulation for the discrete-variable quantum system is the key new theoretical result of the Focus Article. When the Wigner function Equation (14) is used for the nuclear DOFs, where $\widehat{K}_{\rm nuc}(\mathbf{x},\mathbf{p}) = \widehat{K}^{-1}_{\rm nuc}(\mathbf{x},\mathbf{p})$, Equation (4) is then identical to Equation (5) when $\widehat{A} = \widehat{B}$. The mapping Hamiltonian for the quantum Hamiltonian operator Equation (1) produced by either of Equations (4) and (5) leads to the same expression as Equation (34). When the mapping Hamiltonian is utilized to produce the trajectory-based dynamics for a composite system, it is denoted as the weighted mapping model (wMM) approach. The frozen nuclei limit is satisfied in wMM.

Many choices are possible for the discrete or continuous version of the normalized quasi-probability distribution function $w(\gamma)$ in the weighted constraint phase space mapping theory. In the Focus Article, we consider only the simplest cases of the discrete version. When but a single value of parameter $\gamma$ is chosen in Equation (39), that is, $w(\gamma) = \delta(\gamma - \gamma_1)$, we obtain

$$F\gamma^2 + 2\gamma = 1, \tag{41}$$

of which the physical solution is

$$\gamma = \frac{\sqrt{1+F}-1}{F}. \tag{42}$$

Equation (42) is a trivial result that was used in References.[57,114,115,117,197] In this case, the weighted constraint phase space formulation is identical to the constraint phase space formulation, and wMM becomes CMM with Equation (42) when trajectory-based dynamics is considered. When only two values of parameter are selected, that is,

$$w(\gamma) = \sum_{j=1}^{2} w\left(\gamma_j\right)\delta\left(\gamma - \gamma_j\right), \tag{43}$$

Equations (36) and (39) lead to

$$\begin{aligned} w(\gamma_1) &= \frac{1-\chi(\gamma_2)}{\chi(\gamma_1)-\chi(\gamma_2)} \\ w(\gamma_2) &= \frac{\chi(\gamma_1)-1}{\chi(\gamma_1)-\chi(\gamma_2)}. \end{aligned} \tag{44}$$

When the values of parameter $\gamma$ are close to zero or smaller than zero in region $(-1/F, \infty)$, trajectories produced by the Meyer–Miller mapping Hamiltonian Equation (34) for nonadiabatic molecular dynamics are stable. For demonstration in the paper, we choose

$$\gamma_1 = -\gamma_2 = \Delta \tag{45}$$

with $\Delta$ a reasonably small positive real number in region $(0,\ 1/F)$. Figure 3 presents the constraint coordinate-momentum phase space formulation when a single value of parameter $\gamma$ is used (Figure 3a) as well as the weighted formulation when two values of parameter $\gamma$ suggested by Equation (45) are used (Figure 3b).

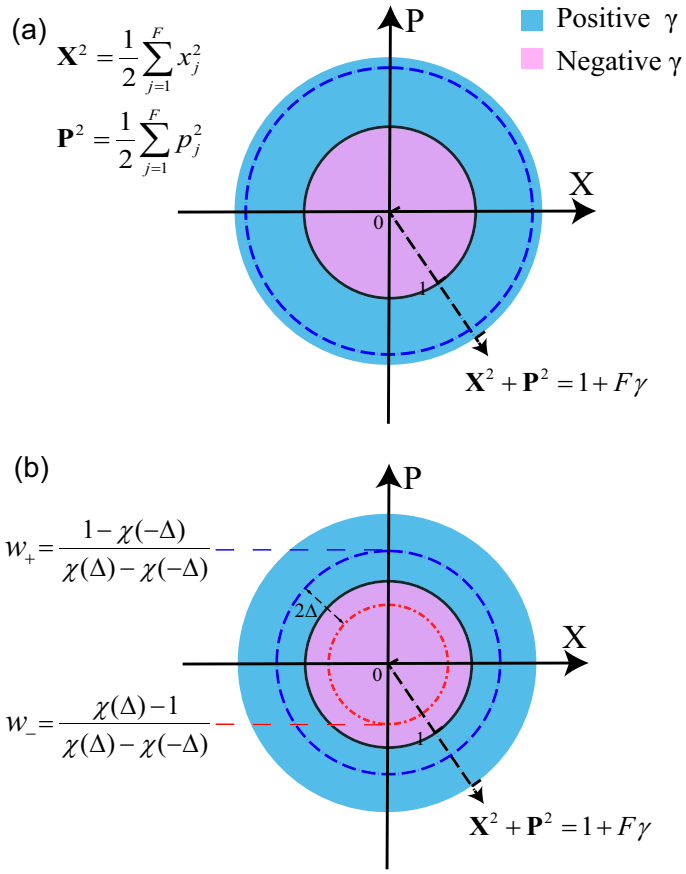


**FIGURE 3** Illustration of the exact mapping formulation with constraint coordinate-momentum phase space. Panel (a) presents constraint phase space with only a single value of parameter $\gamma$. Panel (b) demonstrates weighted constraint phase space with two values of parameter $\gamma$, where the quasi-probability distribution function is $w(\gamma) = w_+\delta(\gamma - \Delta) + w_-\delta(\gamma + \Delta)$. Constraint phase space with the positive weight is blue-dashed, while that with the negative weight is red dot-dashed. (Panel (a) is reprinted with permission from Reference 134, Copyright 2021, American Chemical Society).

## 3 | PHASE SPACE REPRESENTATION OF THE NONCLASSICAL FEATURE OF QUANTUM SYSTEMS

Recent advance in quantum technologies makes it possible to control and manipulate quantum states in experiment. Because the phase space formulation offers an informationally complete description of the density matrix, direct measurements of phase space of the quantum system with continuous DOFs, those of the quantum system with discrete DOFs, and those of the composite quantum system have been realized in experiment.[70,85,221–234] While the celebrated Wigner phase space has long been used for illustration of the negative *quasi*-probability for continuous-variable systems,[225,235] Stratonovich phase space has recently been proposed for visualization and tomography of discrete-variable systems.[85,113,227–229,231,236,237] A combination of these two spaces has been used for illustration of nonclassical correlations or entanglement between the discrete DOF and the continuous DOF of the composite system.[238,239] (In Appendix 3 of the Supporting Information, we briefly review Stratonovich phase space with an either SU(2) or SU ($F$) structure,[114,300,301] as well as the relationship between Stratonovich phase space and constraint coordinate-momentum phase space as already pointed out in References 57,58.)

As coordinate-momentum phase space is well-established in classical mechanics, the formulation of (weighted) constraint coordinate-momentum phase space described in Section 2 offers a potentially useful approach for describing correlations and dynamics in the discrete-variable system as well as the composite system in quantum mechanics. When (weighted) constraint coordinate-momentum phase space is used for mapping an $F$-state system, the phase space distribution is

$$\rho_C(\mathbf{x},\mathbf{p}) = \sum_{m,n=1}^{F} \rho_{mn} K_{nm}(\mathbf{x},\mathbf{p}), \tag{46}$$

where $\rho_{mn} = \langle m|\widehat{\rho}|n\rangle$ and $K_{nm}(\mathbf{x},\mathbf{p}) = \langle n|\widehat{K}_{\text{ele}}(\mathbf{x},\mathbf{p})|m\rangle$ with $\widehat{K}_{\text{ele}}(\mathbf{x},\mathbf{p})$ defined in Equation (38). For the sake of visualization, it is convenient to further reduce constraint phase space variables $(\mathbf{x},\mathbf{p})$ to two relevant variables, $\left(x^{(n)},x^{(m)}\right)$ or $\left(x^{(n)},p^{(m)}\right)$ for describing the correlation on arbitrary two states $|n\rangle$ and $|m\rangle$. We define the marginal function, $\mathcal{K}_{(n,m)}\left(x^{(n)},x^{(m)}\right)$, on constraint coordinate-momentum phase space (Figure 4),

$$\mathcal{K}_{(n,m)}\left(x^{(n)},x^{(m)}\right) = \int F\mathrm{d}\mathbf{x}_{\perp}\,\mathrm{d}\mathbf{p}\frac{1}{\Omega(\gamma)}\delta\left(\sum_{j=1}^{F}\frac{\left(x^{(j)}\right)^2+\left(p^{(j)}\right)^2}{2}-(1+F\gamma)\right)K_{nm}(\mathbf{x},\mathbf{p};\gamma), \tag{47}$$

where $\mathbf{x}_{\perp}$ represents all $x^{(i)}$ other than $\left\{x^{(n)},x^{(m)}\right\}$, and that on weighted constraint phase space,

$$\mathcal{K}_{(n,m)}\left(x^{(n)},x^{(m)}\right) = \int_{-1/F}^{\infty}\mathrm{d}\gamma w(\gamma)\frac{1}{\Omega(\gamma)}\int F\mathrm{d}\mathbf{x}_{\perp}\,\mathrm{d}\mathbf{p}\delta\left(\sum_{j=1}^{F}\frac{\left(x^{(j)}\right)^2+\left(p^{(j)}\right)^2}{2}-(1+F\gamma)\right)K_{nm}(\mathbf{x},\mathbf{p};\gamma). \tag{48}$$

Figure 5 demonstrates the case of Equation (48) when the quasi-probability distribution function $w(\gamma)$ is defined by Equations (43)–(45) where two symmetrical values of parameter $\gamma$ are used. Similar definitions are also applied for $\mathcal{K}_{(n,m)}\left(x^{(n)},p^{(m)}\right)$. The explicit formula of these marginal functions can be derived by using the integral techniques (where we use Wick's theorem)[297,298] in Appendix 1 of the Supporting Information.

Figures 4 and 5 demonstrate a composite system that consists of a discrete DOF for spin-1/2 and a continuous DOF for a harmonic oscillator. The marginal joint distribution function of the composite system reads

$$\rho_C^{(n,m)}\left(\mathbf{R},\mathbf{P};x^{(n)},x^{(m)}\right) = \mathrm{Tr}_{n,e}\left[\widehat{\rho}\widehat{K}_{nuc}(\mathbf{R},\mathbf{P})\bigotimes|n\rangle\langle m|\mathcal{K}_{(n,m)}\left(x^{(n)},x^{(m)}\right)\right]. \tag{49}$$

The marginal quasi-probability distribution functions of the continuous variable for both the pure state and the mixed state are presented in Figure 4a, where infinite Wigner phase space is employed. The marginal functions of the discrete variables (based on Equation (47)) of the spin-1/2 system read

$$\begin{aligned}&\begin{pmatrix}\mathcal{K}_{\uparrow\uparrow}\left(x^{(1)},x^{(2)}\right) & \mathcal{K}_{\uparrow\downarrow}\left(x^{(1)},x^{(2)}\right)\\ \mathcal{K}_{\downarrow\uparrow}\left(x^{(1)},x^{(2)}\right) & \mathcal{K}_{\downarrow\downarrow}\left(x^{(1)},x^{(2)}\right)\end{pmatrix}\\ =&\frac{1}{2\pi(1+2\gamma)}\begin{pmatrix}1+\frac{1}{2}\left(x^{(1)}\right)^2-\frac{1}{2}\left(x^{(2)}\right)^2 & x^{(1)}x^{(2)}\\ x^{(1)}x^{(2)} & 1-\frac{1}{2}\left(x^{(1)}\right)^2+\frac{1}{2}\left(x^{(2)}\right)^2\end{pmatrix},\end{aligned} \tag{50}$$

where notations $\uparrow,\downarrow$ are used to represent the two discrete states.

The marginal functions for the discrete variable are demonstrated on constraint coordinate-momentum phase space in Figure 4b and on weighted constraint space in Figure 5b. More interestingly, the identical angular behavior and the radial cancellation behavior of two weighted components lead to a hollow ring structure on weighted constraint phase space (Figure 5a, also see Appendix 4 of the Supporting Information). The difference between the Schrodinger cat state and the mixed state is distinct in either Figure 4b on constraint space or Figure 5b on weighted constraint space.

The marginal joint function of a pure Bell entangled state, $\left(|0\rangle|\downarrow\rangle+|1\rangle|\uparrow\rangle\right)/2$, of the composite system is demonstrated in Figure 4c (by adopting the similar strategy of References 238,239), where constraint coordinate-momentum phase space is used for the discrete DOF at each grid, as well as in Figure 5c where weighted constraint space is employed for the discrete DOF at each grid. The two-dimensional grids represent variables $(R,P)$ of infinite Wigner phase space for the continuous DOF in either of Figures 4c and 5c. When the pure Bell entangled state is studied, both Figures 4c and 5c clearly demonstrate a Gaussian decay of the joint marginal function against Wigner phase space

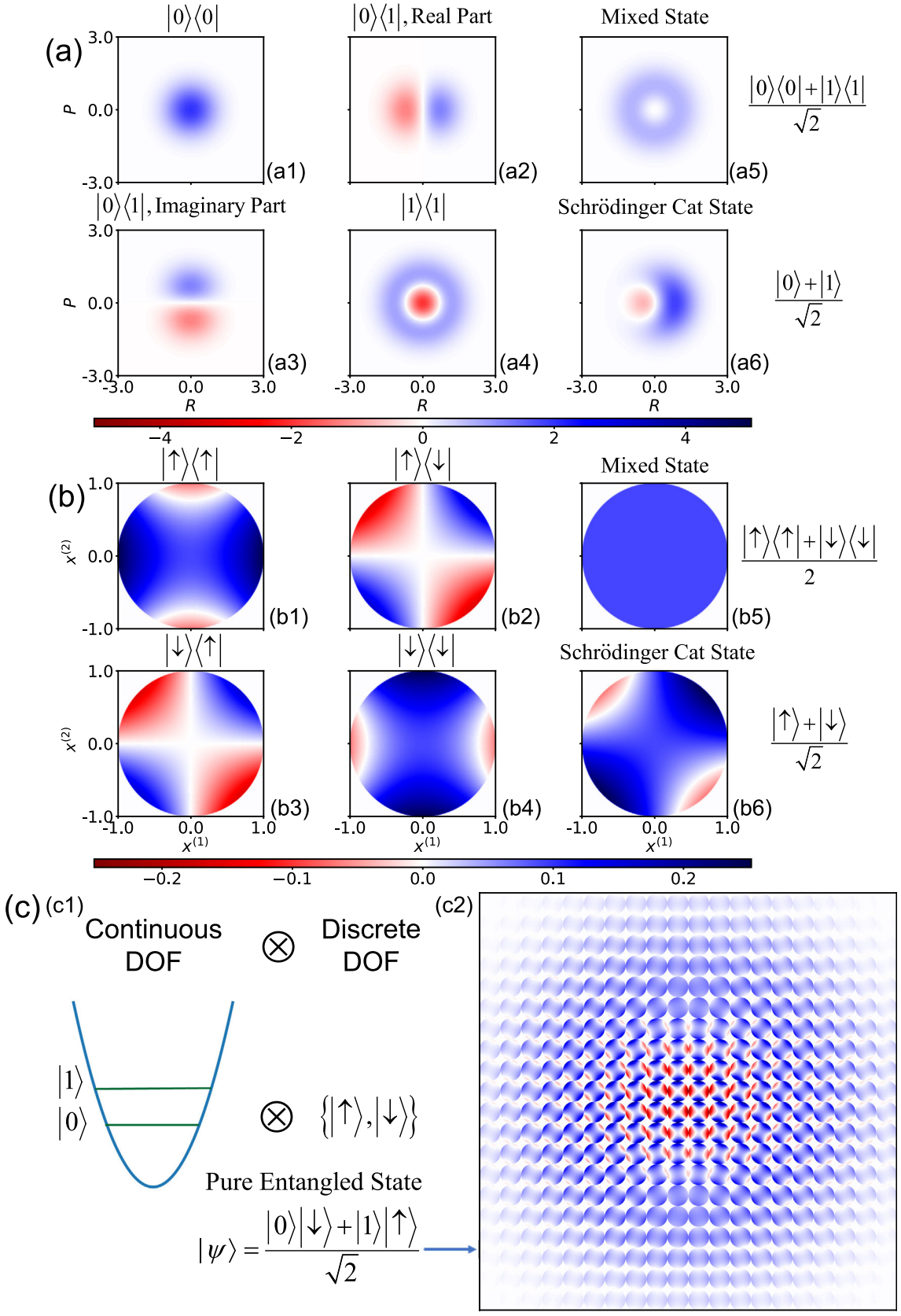


FIGURE 4 Legend on next page.

variables $(R,P)$ of the continuous DOF. Either Figures 4c or 5c also shows the pattern of the correlation between the continuous DOF and the discrete DOF. It is convenient to distinguish the pure Bell entangled state, $\left(|0\rangle|\downarrow\rangle+|1\rangle|\uparrow\rangle\right)/2$, from the direct product of the Schrodinger cat states, $\left(|0\rangle+|1\rangle\right)\otimes\left(|\uparrow\rangle+|\downarrow\rangle\right)/2$, when the hybrid representation of the general coordinate-momentum phase space is used.

## 4 | DYNAMICS OF COMPOSITE QUANTUM SYSTEMS

The quantum Liouville theorem can be expressed as a generalized Moyal bracket on hybrid coordinate-momentum phase space. When the Poisson bracket for classical Hamilton's EOMs governed by the mapping Hamiltonian, Equation (34), is used to approximate the generalized Moyal bracket on phase space,[57,58] we have CMM when constraint space is used, and wMM when weighted constraint space is employed. (Please see Appendices 2, 3, and 5 of the Supporting Information for more discussion.) We compare the new wMM and CMM approaches to Ehrenfest dynamics[240,241] as well as the fewest-switches surface hopping (FSSH) method,[242–244] two prevailing trajectory-based dynamics methods for a few typical composite quantum systems. (In this section we set $\hbar=1$ for simplicity if it is not specifically stated).

### 4.1 | Equations of motion governed by the mapping Hamiltonian

In Equation (1), the "complete" set of diabatic states $\{|n\rangle\}$ is independent of nuclear coordinate/configuration $\mathbf{R}$. The mapping variables for discrete (electronic) DOFs, $(\mathbf{x},\mathbf{p})$, are independent of $\mathbf{R}$. Define $\mathbf{g}=\mathbf{x}+i\mathbf{p}$. The EOMs governed by Equation (33), the mapping Hamiltonian of Equation (1), then read,

$$\dot{\mathbf{g}}=-i\mathbf{V}(\mathbf{R})\mathbf{g} \tag{51}$$

$$\dot{\mathbf{R}}=\mathbf{M}^{-1}\mathbf{P} \tag{52}$$

$$\dot{\mathbf{P}}=-\sum_{n,m=1}^{F}\left(\nabla_{\mathbf{R}}V_{mn}(\mathbf{R})\right)\left(\frac{1}{2}\left(x^{(n)}+ip^{(n)}\right)\left(x^{(m)}-ip^{(m)}\right)-\gamma\delta_{nm}\right). \tag{53}$$

Diabatic potential matrix $\mathbf{V}(\mathbf{R})$ is Hermitian, so is the force matrix, $\{\nabla_{\mathbf{R}}V_{mn}(\mathbf{R})\}$. It is trivial to verify that the mean force of the right-hand side (RHS) of Equation (53) is always real. When $\mathbf{V}(\mathbf{R})$ is a real symmetric matrix, the EOMs become

$$\begin{aligned}\dot{\mathbf{x}}&=\mathbf{V}(\mathbf{R})\mathbf{p}\\ \dot{\mathbf{p}}&=-\mathbf{V}(\mathbf{R})\mathbf{x}\\ \dot{\mathbf{R}}&=\mathbf{M}^{-1}\mathbf{P}\\ \dot{\mathbf{P}}&=-\sum_{n,m=1}^{F}\left(\nabla_{\mathbf{R}}V_{mn}(\mathbf{R})\right)\left[\frac{1}{2}\left(x^{(n)}x^{(m)}+p^{(n)}p^{(m)}\right)-\gamma\delta_{nm}\right].\end{aligned} \tag{54}$$

**FIGURE 4** Illustrations of (a) Wigner representation of a continuous-variable system, (b) constraint phase space representation of a discrete-variable system, and (c) hybrid coordinate-momentum phase space representation of a composite system with both discrete and continuous DOFs. (a) Wigner distribution for $|0\rangle\langle 0|$ (Panel a1), that for $|1\rangle\langle 1|$ (Panel a4), real part (Panel a2) and imaginary part (Panel a3) of the Wigner distribution for $|0\rangle\langle 1|$, Wigner distribution for mixed state $\left(|0\rangle\langle 0|+|1\rangle\langle 1|\right)/2$ (Panel a5), and that for Schrödinger cat state $\left(|0\rangle+|1\rangle\right)/\sqrt{2}$ (Panel a6). Here, $|0\rangle$ and $|1\rangle$ are two energy levels of a continuous-variable system. (b) Marginal distribution of constraint phase space coordinates $\left(x^{(1)},x^{(2)}\right)$ for $|\uparrow\rangle\langle\uparrow|$ (Panel b1), $|\downarrow\rangle\langle\downarrow|$ (Panel b4), that for $|\uparrow\rangle\langle\downarrow|$ (Panel b2), that for $|\downarrow\rangle\langle\uparrow|$ (Panel b3), that for mixed state $\left(|\uparrow\rangle\langle\uparrow|+|\downarrow\rangle\langle\downarrow|\right)/2$ (Panel b5), and that for Schrödinger cat state $\left(|\uparrow\rangle+|\downarrow\rangle\right)/\sqrt{2}$ (Panel b6). Here, $|\uparrow\rangle$ and $|\downarrow\rangle$ represent two discrete states of a discrete-variable system. (c) Panel c1: Schematic representaton of the composite system and the pure entangled state $\left(|0\rangle|\downarrow\rangle+|1\rangle|\uparrow\rangle\right)/2$; Panel c2: hybrid coordinate-momentum phase space representation of the entangled state. The grid is on the Wigner phase space $(R,P)$ for the continous DOF, and each circle of a grid stands for the local marginal distribution function of constraint phase space variables $\left(x^{(1)},x^{(2)}\right)$. The notations are identical to those in Panels (a) and (b).

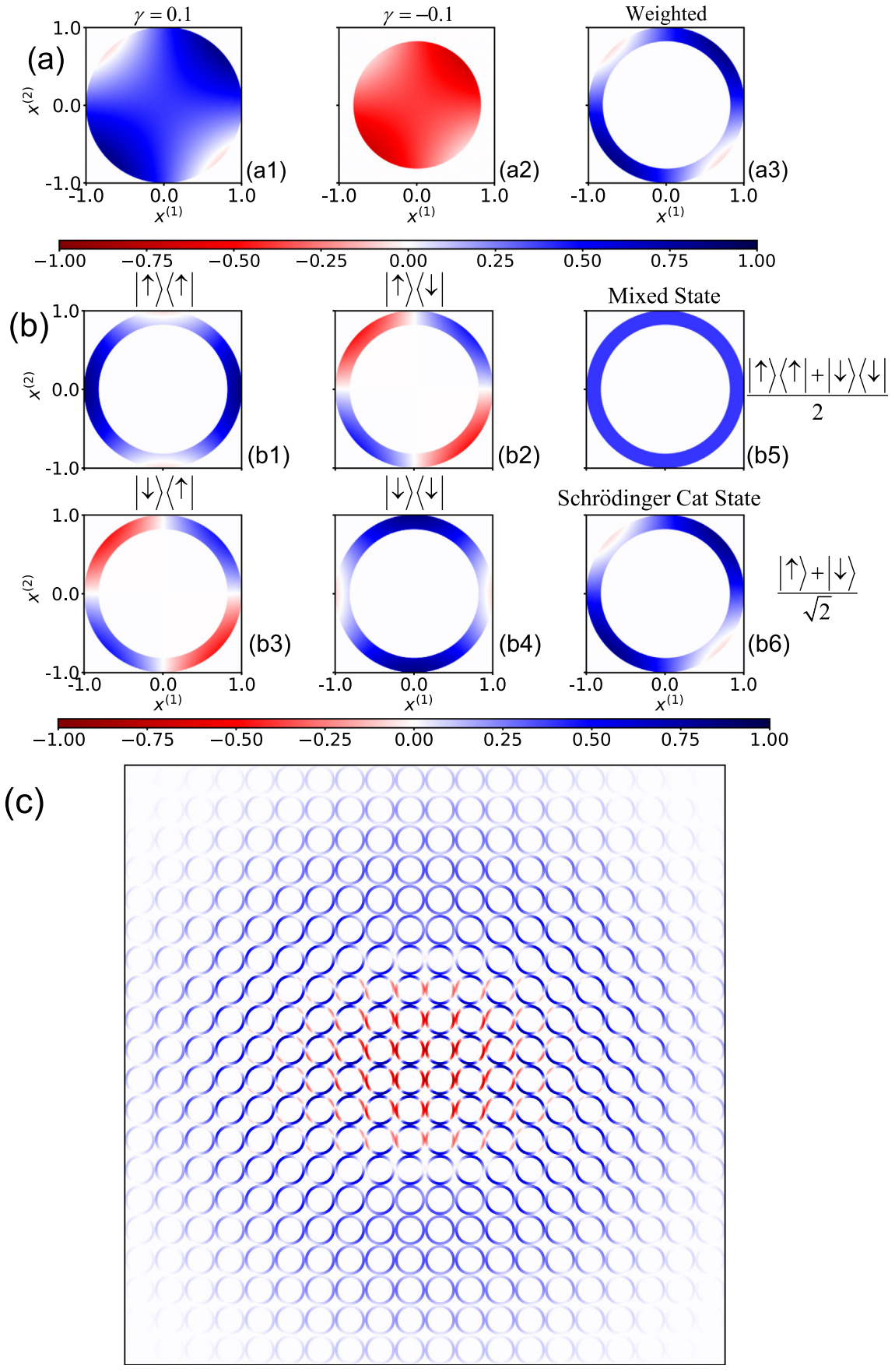


FIGURE 5 Legend on next page.

Consider the full Hamiltonian of nuclei and electrons of the molecular system,

$$\widehat{H} = \frac{1}{2}\widehat{\mathbf{P}}^T \mathbf{M}^{-1}\widehat{\mathbf{P}} + \widehat{H}_{el}\left(\widehat{\mathbf{R}}\right), \tag{55}$$

where $\widehat{H}_{el}\left(\widehat{\mathbf{R}}\right)$ is the electronic Hamiltonian. Its representation in the diabatic basis reads

$$\widehat{H}_{el}(\mathbf{R}) = \sum_{n,m} V_{nm}(\mathbf{R})|n\rangle\langle m|, \tag{56}$$

and that in the adiabatic basis is

$$\widehat{H}_{el}(\mathbf{R}) = \sum_{k} E_k(\mathbf{R})|\phi_k(\mathbf{R})\rangle\langle\phi_k(\mathbf{R})|, \tag{57}$$

where $E_k(\mathbf{R})$ denotes the adiabatic potential energy surface of the $k$-th adiabatic electronic state. Assume that the unitary transformation between a set of diabatic basis states, $\{|m\rangle\}$, and a set of adiabatic basis states, $\{|\phi_k(\mathbf{R})\rangle\}$, is

$$\begin{aligned} |\phi_k(\mathbf{R})\rangle &= \sum_m U_{mk}(\mathbf{R})|m\rangle \\ |n\rangle &= \sum_k U^*_{nk}(\mathbf{R})|\phi_k(\mathbf{R})\rangle, \end{aligned} \tag{58}$$

where $U_{mk}(\mathbf{R}) = \langle m|\phi_k(\mathbf{R})\rangle$. This states the diagonalization of the diabatic potential matrix,

$$\sum_{n,m} U^*_{nj}(\mathbf{R})V_{nm}(\mathbf{R})U_{mk}(\mathbf{R}) = E_k(\mathbf{R})\delta_{kj}, \tag{59}$$

or equivalently,

$$V_{mn}(\mathbf{R}) = \sum_k U_{mk}(\mathbf{R})E_k(\mathbf{R})U^*_{nk}(\mathbf{R}). \tag{60}$$

Define the nonadiabatic coupling vector,

$$\mathbf{d}_{mn}(\mathbf{R}) = \langle\phi_m(\mathbf{R})\left|\frac{\partial\phi_n(\mathbf{R})}{\partial\mathbf{R}}\right\rangle. \tag{61}$$

It is trivial to show

$$\mathbf{d}_{mn}(\mathbf{R}) = -\mathbf{d}^*_{nm}(\mathbf{R}), \tag{62}$$

because of the orthonormality of the basis set, that is, $\langle\phi_m(\mathbf{R})|\phi_n(\mathbf{R})\rangle = \delta_{mn}$. We then obtain

**FIGURE 5** Illustrations of (a) components and (b) marginal distribution functions of the weighted constraint phase space representation of a discrete-variable system, and (c) weighted hybrid representation of the same composite system as that of Figure 4c. (a) Marginal distribution of constraint phase space coordinates $\left(x^{(1)},x^{(2)}\right)$ for Schrödinger cat state $\left(|\uparrow\rangle+|\downarrow\rangle\right)/\sqrt{2}$ with $\gamma=\Delta$ weighted by $w_+$ (Panel a1), with $\gamma=-\Delta$ weighted by $w_-$ (Panel a2). The sum of the two components yields the marginal distribution of constraint phase space coordinates $(x_1,x_2)$ of the weighted representation with two values of parameter $\gamma$ for the Schrödinger cat state (Panel a3). Coordinates are scaled by the larger radius $\sqrt{2(1+2\Delta)}$. (b) Weighted marginal distribution of constraint phase space coordinates $\left(x^{(1)},x^{(2)}\right)$ for the same properties as those in Figure 4b. (c) Same as Figure 4c, but using weighted marginal distribution for the discrete DOF.

$$\begin{aligned}\nabla_{\mathbf{R}} U^*_{mk}(\mathbf{R}) &= \langle \nabla_{\mathbf{R}} \phi_k(\mathbf{R}) | m \rangle = \sum_n \langle \nabla_{\mathbf{R}} \phi_k(\mathbf{R}) | \phi_n \rangle \langle \phi_n | m \rangle \\ &= \sum_n \mathbf{d}^*_{nk}(\mathbf{R}) U^*_{mn}(\mathbf{R}) = -\sum_n \mathbf{d}_{kn}(\mathbf{R}) U^*_{mn}(\mathbf{R})\end{aligned} \tag{63}$$

and

$$\nabla_{\mathbf{R}} U_{mk}(\mathbf{R}) = -\sum_n \mathbf{d}^*_{kn}(\mathbf{R}) U_{mn}(\mathbf{R}) = \sum_n U_{mn}(\mathbf{R}) \mathbf{d}_{nk}(\mathbf{R}). \tag{64}$$

Below we show the explicit form of the EOMs, Equations (51)–(53), under the diabatic-to-adiabatic transformation, Equation (58).

The covariant transformation for mapping variables corresponding to the diabatic-to-adiabatic transformation, Equation (58), reads

$$\widetilde{x}^{(n)}(\mathbf{R}) + i\widetilde{p}^{(n)}(\mathbf{R}) = \sum_m U^*_{mn}(\mathbf{R}) \left( x^{(m)} + i p^{(m)} \right) \tag{65}$$

or

$$x^{(n)} + i p^{(n)} = \sum_m U_{nm}(\mathbf{R}) \left( \widetilde{x}^{(m)}(\mathbf{R}) + i\widetilde{p}^{(m)}(\mathbf{R}) \right). \tag{66}$$

Denote $\widetilde{\mathbf{g}}(\mathbf{R}) = \widetilde{\mathbf{x}}(\mathbf{R}) + i\widetilde{\mathbf{p}}(\mathbf{R})$. Equations (65)–(66) become

$$\begin{aligned}\widetilde{\mathbf{g}}(\mathbf{R}) &= \mathbf{U}^\dagger(\mathbf{R}) \mathbf{g} \\ \mathbf{g} &= \mathbf{U}(\mathbf{R}) \widetilde{\mathbf{g}}(\mathbf{R}).\end{aligned} \tag{67}$$

The electronic mapping kernel, Equation (29), is

$$\widehat{K}_{\text{ele}} = \sum_{n,m} \left[ \frac{1}{2} \left( \widetilde{x}^{(n)} + i\widetilde{p}^{(n)} \right) \left( \widetilde{x}^{(m)} - i\widetilde{p}^{(m)} \right) - \gamma \delta_{nm} \right] |\phi_n\rangle\langle\phi_m|, \tag{68}$$

under the transformation for a specific nuclear configuration, $\mathbf{R}$. Substitution of Equation (63) into Equation (65) yields

$$\nabla_{\mathbf{R}} \left( \widetilde{x}^{(n)}(\mathbf{R}) + i\widetilde{p}^{(n)}(\mathbf{R}) \right) = -\sum_k \mathbf{d}_{nk}(\mathbf{R}) \left( \widetilde{x}^{(k)}(\mathbf{R}) + i\widetilde{p}^{(k)}(\mathbf{R}) \right). \tag{69}$$

The total time derivative of $\widetilde{x}^{(n)} + i\widetilde{p}^{(n)}$ reads

$$\begin{aligned}\frac{\mathrm{d}}{\mathrm{d}t} \left( \widetilde{x}^{(n)} + i\widetilde{p}^{(n)} \right) &= \sum_m U^*_{mn}(\mathbf{R}) \left( \frac{\mathrm{d}}{\mathrm{d}t} \left( x^{(m)} + i p^{(m)} \right) \right) + \sum_m \left( \frac{\mathrm{d}}{\mathrm{d}t} U^*_{mn}(\mathbf{R}) \right) \left( x^{(m)} + i p^{(m)} \right) \\ &= -i \sum_k \delta_{nk} E_k(\mathbf{R}) \left( \widetilde{x}^{(k)} + i\widetilde{p}^{(k)} \right) - \sum_k \dot{\mathbf{R}} \cdot \mathbf{d}_{nk}(\mathbf{R}) \left( \widetilde{x}^{(k)} + i\widetilde{p}^{(k)} \right) \\ &= -i \sum_k \left[ E_k(\mathbf{R}) \delta_{nk} - i\dot{\mathbf{R}} \cdot \mathbf{d}_{nk}(\mathbf{R}) \right] \left( \widetilde{x}^{(k)} + i\widetilde{p}^{(k)} \right).\end{aligned} \tag{70}$$

Equation (70) is the EOMs for mapping variables of electronic DOFs in the adiabatic representation.

We then consider the EOMs of nuclear mapping variables under the transformation Equation (58). Equation (52) remains invariant under the transformation. Substitution of Equations (60), (63), (64), and (69) into Equation (53) produces

$$\begin{aligned}\dot{\mathbf{P}} &= -\sum_{n,m=1}^{F}(\nabla_{\mathbf{R}}V_{mn}(\mathbf{R}))\left[\frac{1}{2}\left(x^{(n)}+ip^{(n)}\right)\left(x^{(m)}-ip^{(m)}\right)-\gamma\delta_{nm}\right]\\ &= -\sum_{n,m}\nabla_{\mathbf{R}}\left(\sum_{k}U_{mk}(\mathbf{R})E_k(\mathbf{R})U^{*}_{nk}(\mathbf{R})\right)\left[\frac{1}{2}\left(x^{(n)}+ip^{(n)}\right)\left(x^{(m)}-ip^{(m)}\right)-\gamma\delta_{nm}\right]\\ &= \sum_{k,l}\mathbf{d}_{lk}(\mathbf{R})(E_l(\mathbf{R})-E_k(\mathbf{R}))\left[\frac{1}{2}\left(\tilde{x}^{(k)}+i\tilde{p}^{(k)}\right)\left(\tilde{x}^{(l)}-i\tilde{p}^{(l)}\right)-\gamma\delta_{kl}\right]\\ &\quad -\sum_{k,l}\nabla_{\mathbf{R}}E_k(\mathbf{R})\delta_{kl}\left[\frac{1}{2}\left(\tilde{x}^{(k)}+i\tilde{p}^{(k)}\right)\left(\tilde{x}^{(l)}-i\tilde{p}^{(l)}\right)-\gamma\delta_{kl}\right].\end{aligned} \tag{71}$$

Since force matrix $\{\mathbf{F}_{kl}=\nabla_{\mathbf{R}}E_k(\mathbf{R})\delta_{kl}+(E_k(\mathbf{R})-E_l(\mathbf{R}))\mathbf{d}_{lk}(\mathbf{R})\}$ is Hermitian, the mean force of the RHS of Equation (71) stays real. Under the diabatic-to-adiabatic transformation, Equation (58), the EOMs of nuclear phase variables (Equations (52) and (53)) are then recast into

$$\begin{aligned}\dot{\mathbf{R}} &= \mathbf{M}^{-1}\mathbf{P}\\ \dot{\mathbf{P}} &= -\sum_{k,l}[\nabla_{\mathbf{R}}E_k(\mathbf{R})\delta_{kl}+(E_k(\mathbf{R})-E_l(\mathbf{R}))\mathbf{d}_{lk}(\mathbf{R})]\left[\frac{1}{2}\left(\tilde{x}^{(k)}+i\tilde{p}^{(k)}\right)\left(\tilde{x}^{(l)}-i\tilde{p}^{(l)}\right)-\gamma\delta_{kl}\right].\end{aligned} \tag{72}$$

Define the effective potential matrix, $\mathbf{V}^{(\mathrm{eff})}$, whose element is a function of the nuclear phase variables,

$$V^{(\mathrm{eff})}_{nk}(\mathbf{R},\mathbf{P}) = E_n(\mathbf{R})\delta_{nk} - i\dot{\mathbf{R}}\cdot\mathbf{d}_{nk}(\mathbf{R}) = E_n(\mathbf{R})\delta_{nk} - i\mathbf{M}^{-1}\mathbf{P}\cdot\mathbf{d}_{nk}(\mathbf{R}). \tag{73}$$

A more compact form of Equation (70) for the electronic phase variables becomes

$$\dot{\tilde{\mathbf{g}}} = -i\mathbf{V}^{(\mathrm{eff})}(\mathbf{R},\mathbf{P})\tilde{\mathbf{g}}. \tag{74}$$

Equations (72) and (74) are the final EOMs under the covariant transformation Equation (65).

When the electronic wavefunction of the basis set is always real, that is, $\langle r|\phi_n(\mathbf{R})\rangle$ is real for any $n$, which is often the case for molecular systems, Equation (62) leads to

$$\mathbf{d}_{mn}(\mathbf{R}) = -\mathbf{d}_{nm}(\mathbf{R}). \tag{75}$$

Equation (72) is simplified to

$$\begin{aligned}\dot{\mathbf{R}} &= \mathbf{M}^{-1}\mathbf{P}\\ \dot{\mathbf{P}} &= -\sum_{k,l}[\nabla_{\mathbf{R}}E_k(\mathbf{R})\delta_{kl}+(E_k(\mathbf{R})-E_l(\mathbf{R}))\mathbf{d}_{lk}(\mathbf{R})]\left[\frac{1}{2}\left(\tilde{x}^{(k)}\tilde{x}^{(l)}+\tilde{p}^{(k)}\tilde{p}^{(l)}\right)-\gamma\delta_{kl}\right].\end{aligned} \tag{76}$$

Note that the mapping Hamiltonian of Equation (33) (obtained in the diabatic representation) becomes

$$H_C(\mathbf{R},\mathbf{P},\mathbf{x}(\tilde{\mathbf{x}},\tilde{\mathbf{p}}),\mathbf{p}(\tilde{\mathbf{x}},\tilde{\mathbf{p}})) = \frac{1}{2}\mathbf{P}^T\mathbf{M}^{-1}\mathbf{P} + \sum_{n=1}^{F}E_n(\mathbf{R})\left(\frac{1}{2}\left(\left(\tilde{x}^{(n)}(\mathbf{R})\right)^2+\left(\tilde{p}^{(n)}(\mathbf{R})\right)^2\right)-\gamma\right) \tag{77}$$

under the transformation defined by Equations (60) and (65). The new EOMs, Equations (72) and (74), conserve the mapping Hamiltonian of Equation (77). The diabatic-to-adiabatic transformation depends on nuclear coordinate $\mathbf{R}$, which is also a time-dependent variable of the evolution. The time-dependent canonical transformation for the Hamiltonian system yields a new set of EOMs by the chain rule.[245]

In Equations (71)–(74) and (76)–(77) $\mathbf{P}$ correspond to the mapping momentum in the diabatic representation, but *not* the canonical momentum in the adiabatic representation because Equation (71) is *not* generated from Hamilton's equations of motion. Equations (74) and (76) share a similar form to the EOMs proposed by Cotton et al.[184] and discussed in the Supporting Information of Reference 57. Define the covariant transformation for nuclear phase variables,

$$\begin{aligned} \widetilde{\mathbf{R}} &= \mathbf{R} \\ \widetilde{\mathbf{P}} &= \mathbf{P} + i\sum_{m,n}\left[\frac{1}{2}\left(\tilde{x}^{(n)} + i\tilde{p}^{(n)}\right)\left(\tilde{x}^{(m)} - i\tilde{p}^{(m)}\right) - \gamma\delta_{nm}\right]\mathbf{d}_{mn}(\mathbf{R}). \end{aligned} \tag{78}$$

The Hamiltonian of Equation (77) becomes

$$\begin{aligned} H_C\left(\widetilde{\mathbf{R}},\widetilde{\mathbf{P}},\widetilde{\mathbf{x}},\widetilde{\mathbf{p}}\right) &= \frac{1}{2}\mathbf{P}\left(\widetilde{\mathbf{P}},\widetilde{\mathbf{x}},\widetilde{\mathbf{p}},\widetilde{\mathbf{R}}\right)^T\mathbf{M}^{-1}\mathbf{P}\left(\widetilde{\mathbf{P}},\widetilde{\mathbf{x}},\widetilde{\mathbf{p}},\widetilde{\mathbf{R}}\right) \\ &+ \sum_{n=1}^{F} E_n\left(\widetilde{\mathbf{R}}\right)\left(\frac{1}{2}\left(\left(\tilde{x}^{(n)}\left(\widetilde{\mathbf{R}}\right)\right)^2 + \left(\tilde{p}^{(n)}\left(\widetilde{\mathbf{R}}\right)\right)^2\right) - \gamma\right), \end{aligned} \tag{79}$$

of which the canonical variables are $\left\{\widetilde{\mathbf{R}},\widetilde{\mathbf{P}},\widetilde{\mathbf{x}},\widetilde{\mathbf{p}}\right\}$ instead of $\{\mathbf{R},\mathbf{P},\widetilde{\mathbf{x}},\widetilde{\mathbf{p}}\}$. (See more discussion in Appendix 2 of the Supporting Information). The mapping diabatic momentum, $\mathbf{P}$, is related to the kinematic momentum of the adiabatic representation. Although we can directly use Hamilton's EOMs for $\left\{\widetilde{\mathbf{R}},\widetilde{\mathbf{P}},\widetilde{\mathbf{x}},\widetilde{\mathbf{p}}\right\}$, it is more convenient to employ the EOMs for $\{\mathbf{R},\mathbf{P},\widetilde{\mathbf{x}},\widetilde{\mathbf{p}}\}$ instead to avoid the derivative of nonadiabatic coupling terms. This is indeed the strategy suggested by Cotton et al.[184] When the initial condition does not involve nonadiabatic coupling terms, the sampling of $\mathbf{P}$ in the diabatic representation is the same for that of $\widetilde{\mathbf{P}}$ in the adiabatic representation. This is the case in the following applications, where FSSH has to be used in the adiabatic representation. By applying the covariance relation under the diabatic-to-adiabatic transformation, the EOMs on mapping phase space are independent of the representation of the (electronic) basis set, which is also the merit of Ehrenfest dynamics.

We note that either Equation (51) or Equation (74) can analytically be solved by a symplectic approach that employs an exact propagator on electronic phase space at each nuclear phase point. For example, for Equation (74), we use

$$\widetilde{\mathbf{U}}(\mathbf{R},\mathbf{P};\Delta t) = \exp\left[-i\Delta t\mathbf{V}^{(\mathrm{eff})}\right], \tag{80}$$

such that the evolution of electronic phase variables follows $\widetilde{\mathbf{g}}(t+\Delta t) = \widetilde{\mathbf{U}}(\mathbf{R},\mathbf{P};\Delta t)\widetilde{\mathbf{g}}(t)$.

We then test a range of benchmark systems, including two-site dissipative models, Tully's scattering models, atomic systems in cavity interacted with a number of field modes, and linear vibronic coupling model systems that involve the conical intersection.[135,246–248] They are typical composite quantum systems in chemistry, physics, condensed matter science, quantum optics, and quantum information.

## 4.2 | Spin-boson models at low-temperature in condensed phase

The first model illustrated is the spin-boson model, which describes a two-site system interacted with an environmental bath in the condensed phase. It is also a simplified model for electron transfer and energy transfer in chemical and biological reactions. Several numerically exact benchmark methods for solving the spin-boson model include quasi-adiabatic propagator path integral (QuAPI)[249–252] and more efficient small matrix PI (SMatPI),[304,305] hierarchy equations of motion (HEOM),[253–261] and (multi-layer) multi-configuration time-dependent Hartree [(ML-)MCTDH].[262–268] Quantum dynamics of the spin-boson model exhibits interesting dissipative characters, of which the asymptotic behaviors are

often missed by either of Ehrenfest dynamics and FSSH in the low-temperature regime.[58] Spin-boson models with strong coupling in the low-temperature regime present challenging tests for trajectory-based dynamics methods.

The Hamiltonian of the spin-boson model is divided to three parts, $\widehat{H}=\widehat{H}_s+\widehat{H}_b+\widehat{H}_{sb}$. Here $\widehat{H}_s=\varepsilon\widehat{\sigma}_z+\Delta_c\widehat{\sigma}_x$ describes a two-site system with the bias, $\varepsilon$, and tunneling $\Delta_c$, while the bath part of the Hamiltonian is discretized into a combination of a number of quantum harmonic oscillators $\widehat{H}_b=\sum_{j=1}^{N_b}\left(\widehat{P}_j^2+\omega_j^2\widehat{R}_j^2\right)/2$. The system-bath coupling adopts a bilinear interaction, $\widehat{H}_{sb}=-\sum_{j=1}^{N_b}c_j\widehat{R}_j\widehat{\sigma}_z$. Here, we use an Ohmic bath spectral density $J(\omega)=(\pi/2)\alpha\omega e^{-\omega/\omega_c}$, where $\alpha$ is the Kondo parameter and $\omega_c$ is the cut-off frequency. Its discrete frequencies and coupling strengths $\{\omega_j,c_j\}$ are sampled[269,270,306] from

$$\begin{cases}\omega_j=-\omega_c\ln[1-j/(1+N_b)]\\ c_j=\omega_j\sqrt{\alpha\omega_c/(1+N_b)}\end{cases},\quad j=1,\ldots,N_b. \tag{81}$$

The initial density is set as $|1\rangle_s\langle 1|_s\otimes\widehat{\rho}_b$, where the system is in excited state $|1\rangle_s$ while all bath modes are at thermal equilibrium with $\widehat{\rho}_b=e^{-\beta H_b}/Z_b$. Initial nuclear DOFs are sampled from the Wigner distribution of $\widehat{\rho}_b$, while initial electronic DOFs are sampled from (weighted) constraint coordinate-momentum phase space $\mathcal{S}(\mathbf{x},\mathbf{p})$. The continuous spectral density is discretized into $N_b=300$ effective bath modes to guarantee numerical convergence in simulations.

In Figure 6, we demonstrate results produced by wMM with parameter $\Delta=0.05$, by wMM with $\Delta=0.1$, and by CMM with $\gamma=\left(\sqrt{F+1}-1\right)/F=0.366$ that is a special case of CMM of Reference 134. Numerically exact results, as well as results yielded by Ehrenfest dynamics and FSSH, are also shown for comparison. Figure 6 indicates that wMM, as well as CMM, outperforms both Ehrenfest dynamics and FSSH dynamics, either for short-time coherences or for long-time dissipations.

## 4.3 | Tully's gas phase scattering models

Tully's scattering models[242] mimic different intersection types of molecular systems, which have widely been tested for various nonadiabatic dynamics methods. They describe a two-state Hamiltonian with a central coupling area and asymptotic plateau regions where diabatic potential function $V_{nn}(R\to\pm\infty)$ is flat. All the three models, including the single avoided crossing (SAC), dual avoided crossing (DAC), and extended coupling region (ECR) problems, are used in our numerical tests.

Atomic units are used in the simulations of the Tully models. The SAC model (Panel a1 of Figure 7) describes the simplest but essential surface crossing in molecular systems. In the diabatic representation, its diagonal potential energy surfaces (PESes) are $V_{11}=-V_{22}=A\left(1-e^{-B|R|}\right)\mathrm{sgn}(R)$ and off-diagonal coupling terms are $V_{12}=V_{21}=Ce^{-DR^2}$. Here, the parameters are $A=0.01$, $B=1.6$, $C=0.005$, and $D=1.0$. The DAC model (Panel b1 of Figure 7) includes two crossing points, thus different (electronic) paths are interfered with the dependence on the initial momentum. Its diagonal PESes are $V_{11}=0$ and $V_{22}=-Ae^{-BR^2}+E_0$, and off-diagonal coupling terms are $V_{12}=V_{21}=Ce^{-DR^2}$ in the diabatic representation with parameters $A=0.10$, $B=0.28$, $E_0=0.05$, $C=0.015$, and $D=0.06$. The ECR model in the diabatic representation (Panel c1 of Figure 7) has diagonal PESes $V_{11}=-V_{22}=E_0$ and coupling terms $V_{12}=V_{21}=C[e^{BR}\Theta(-R)+(2-e^{-BR})\Theta(R)]$, with $E_0=-0.0006$, $B=0.9$, and $C=0.1$. Here, $\Theta(R)$ is the Heaviside function of coordinate $R$. The adiabatic PESes and nonadiabatic coupling vector of the ECR model are also illustrated in Panel c2 of Figure 7.

We investigate the transmission and reflection coefficients of each state. In the simulations, the initial condition is a nuclear wavepacket, $\Psi(R;t=0)\propto\exp\left[-\alpha(R-R_0)^2/2+i(R-R_0)P_0\right]$ (here we adopt $\hbar=1$), occupied in state *1*, where $\alpha=1$ is the Gaussian width parameter, and $R_0$ and $P_0$ are the initial average coordinate and momentum. The initial average coordinate is set at $R_0=-3.8$, $-10$, and $-13$ for the SAC, DAC, and ECR models, respectively. The initial Wigner distribution for the nuclear DOF is then $\rho_{\mathrm{W}}^{\mathrm{nuc}}(R,P)\propto\exp\left[-\alpha(R-R_0)^2-(P-P_0)^2/\alpha\right]$.

Figure 7a shows that all methods are capable of quantitatively describing transmission coefficients in (diabatic) state 1 and state 2 of the SAC model. Figure 7b demonstrates that either wMM or CMM outperforms Ehrenfest dynamics and FSSH in predicting the peak shape when the initial momentum is relatively high, for example, $P_0\geq 15$ au. This indicates that the trajectory-based approximate dynamics approaches in the mapping phase space formulation are good for fast processes in the gas phase composite/nonadiabatic system. However, the performance of either wMM or CMM in the low initial momentum region should be improved. It is important to note that the EOMs of wMM/CMM are

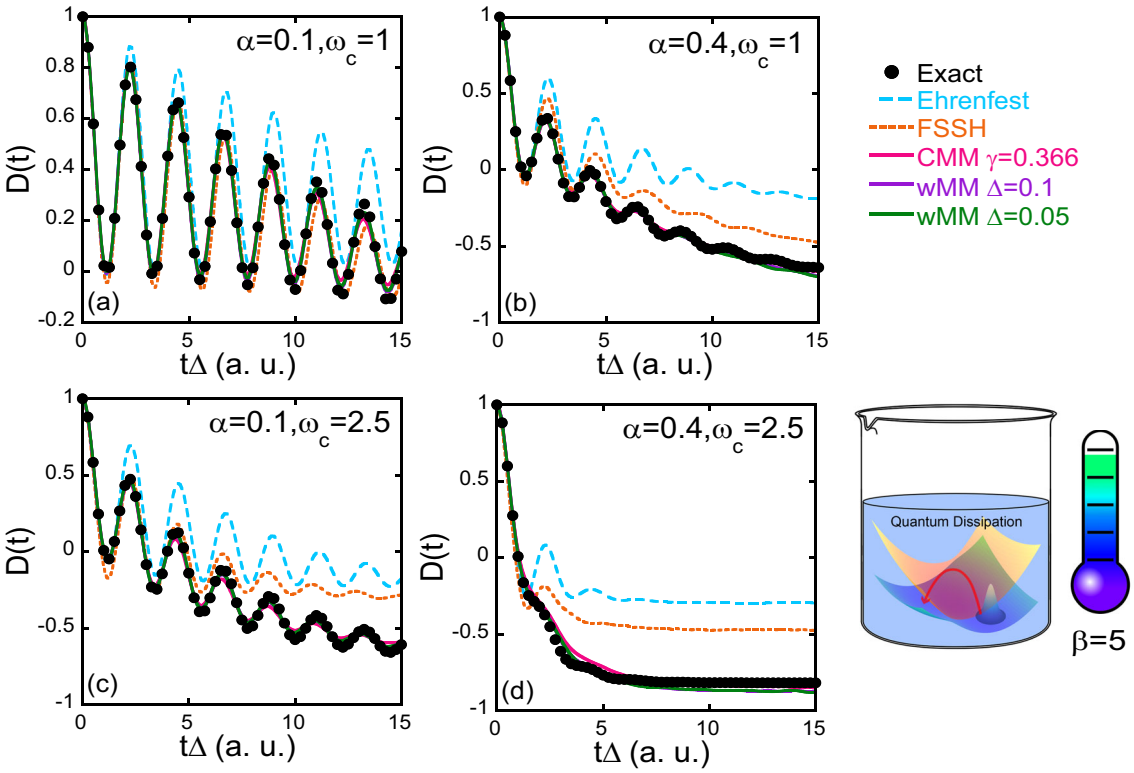


**FIGURE 6** Results of population difference $D(t) = P_1(t) - P_0(t)$ between two states for the spin-boson model at low temperature ($\beta = 1/(k_B T) = 5$) with the Ohmic bath. Panel (a) reports the population dynamics of the spin-boson model with parameters $\varepsilon = \Delta_c = 1$, $\beta = 5, \omega_c = 1, \alpha = 0.1$ in Panel (a). Solid circles: Exact results produced by eHEOM reported in Reference 134. Cyan dashed lines: Ehrenfest dynamics. Orange dashed lines: FSSH. Magenta solid lines: CMM with $\gamma = 0.366$. Purple and green solid lines: wMM with $\Delta = 0.1$ and 0.05, respectively. Panel (b) is similar to Panel (a) but for $\alpha = 0.4$; Panel (c) is similar to Panel (a) but for $\omega_c = 2.5$; Panel (d) is similar to Panel (a) but for $\omega_c = 2.5, \alpha = 0.4$. In each model, 300 continuous DOFs (i.e., effective bath modes) are used.

invariant with the representation of the electronic state, as described in the Supporting Information of Reference 57. (More discussion is also available in Appendix 2 of the Supporting Information.) That is, both the diabatic and adiabatic representations produce the same results for wMM or CMM, which is often not satisfied in FSSH and other nonadiabatic dynamics approaches.

For the ECR model of Figure 7c, the numerically exact DVR solution indicates an energy threshold for a bifurcation. Ehrenfest dynamics totally misses the step-like behaviors for the transmission coefficient in state 1, and for the reflection coefficient in either state 1 or state 2. CMM greatly improves over Ehrenfest dynamics. It is more encouraging that wMM is capable of faithfully describing such step-like behaviors. Tully's original FSSH algorithm is not able to well describe the ECR model,[242] but a modified version for treating frustrated hopping of FSSH (e.g., see Reference244) is capable of qualitatively capturing the step-like behaviors. As shown in Figure 7c, in comparison to the traditional FSSH approach,[242,244] the overall performance of wMM for the ECR model is better.

## 4.4 | Atom/molecule-in-cavity models of quantum electrodynamic light-matter systems

The cavity quantum electrodynamics (cQED) focuses on studying the interaction between light and a multi-level system (e.g., an atom or a molecule) in an optical cavity, which has many applications in the field of quantum information and quantum computation. There exist many interesting and important phenomena in cQED, for example, the Purcell effect when the coupling is weak and the vacuum Rabi splitting when the coupling becomes strong.[271–285] When the general atomic/molecular system is coupled to multi-cavity modes, it is often intractable to solve the exact evolution in real time due to the curse of dimensionality. We test wMM for two typical models that describe an imprisoned multi-level atom coupled with a series of optical modes in a one-dimensional lossless cavity.[57,204,286–289]

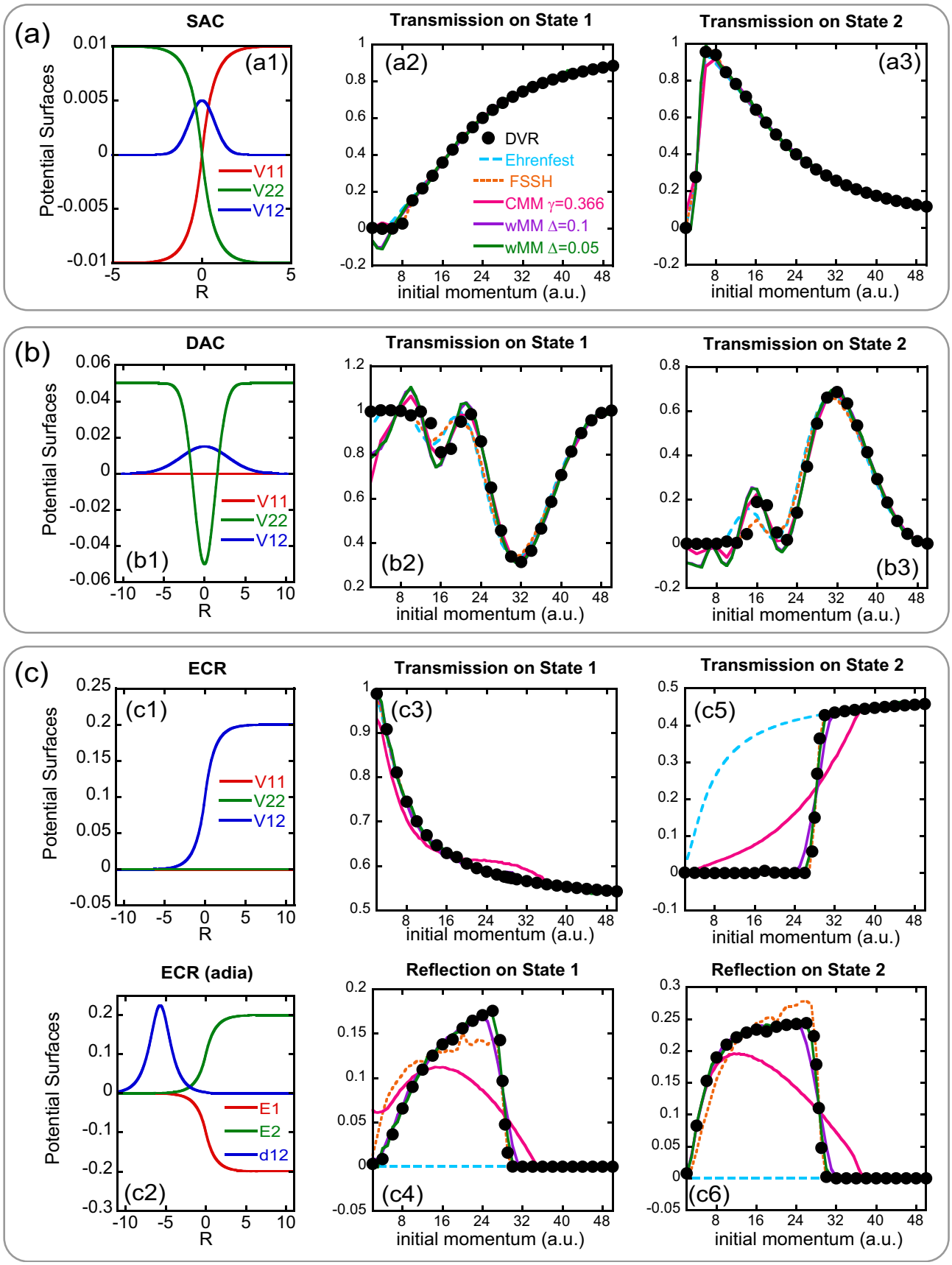


FIGURE 7 Legend on next page.

The total Hamiltonian consists of three parts. The optical field is depicted by $N$ effective modes

$$\widehat{H}_p = \sum_{j=1}^{N} \frac{1}{2}\left(\widehat{P}_j^2 + \omega_j^2 \widehat{R}_j^2\right), \tag{82}$$

where $\left\{\widehat{R}_j, \widehat{P}_j\right\}$ denote the canonical coordinate-momentum variables of $j$-th optical field mode with the corresponding photonic frequency $\omega_j$. The atomic system is described by $\widehat{H}_a = \sum_{n=1}^{F} \varepsilon_n |n\rangle\langle n|$ with $\varepsilon_n$ representing the $n$-th atomic energy level. Employing the dipole approximation, one can formulate the interaction between atom and optical field as

$$\widehat{H}_c = \sum_{n \neq m}^{F} \left( \sum_{j=1}^{N} \omega_j \lambda_j(r_0) \widehat{R}_j \right) \mu_{nm} |n\rangle\langle m|. \tag{83}$$

Here $\mu_{nm}$ denotes the transitional dipole moment between the $n$-th and $m$-th atomic levels, and the coupling between the $j$-th mode and the atom is

$$\lambda_j(r_0) = \sqrt{\frac{2}{\varepsilon_0 L}} \sin\left(\frac{j\pi r_0}{L}\right), \tag{84}$$

where $L$ is the volume length of cavity, $\varepsilon_0$ denotes the vacuum permittivity, and $r_0$ represents the location of the atom. In the simulation, the volume length of the cavity is set to 236,200 au, and the atom is frozen at the central location, that is, $r_0 = L/2$. The optical field is depicted by 400 standing-wave modes in cavity, of which the $j$-th frequency is $\omega_j = j\pi c/L$ with $c$ the light speed in vacuum. We use two benchmark models for studying cQED processes, a three-level model with $\varepsilon_1 = -0.6738$, $\varepsilon_2 = -0.2798$, $\varepsilon_3 = -0.1547$, $\mu_{12} = -1.034$, $\mu_{23} = -2.536$ (all in atomic units), and a reduced two-level model where only the two lowest atomic levels are employed.

The highest atomic level of each model is initially occupied with no photon in cavity, that is, all cavity modes are in the corresponding vacuum state. The spontaneous emission occurs at the beginning, the released photon evolves in the cavity, and the re-absorption and re-emission happen later when the photon is reflected to meet the atom. Figure 8 shows the population transfer of each atomic level of the two models. The wMM results are compared with CMM, Ehrenfest dynamics, FSSH, and exact results.[287,288] Results of Ehrenfest dynamics and of FSSH significantly deviate from exact results even since very short time, while CMM and wMM yield much more reasonable descriptions for all energy levels, including the transfer behavior at short time and the revival at around $t = 1800$ au. The wMM approach shows overall better performance than CMM in most of the cases. Figure 8 implies that the trajectory-based methods in the general coordinate-momentum phase space formulation will be useful for studying cQED phenomena in the field of quantum optics and quantum information.

## 4.5 | Linear vibronic coupling model for the molecular system involving the conical intersection

The conical intersection widely exists in molecular systems and plays a central role in many photophysical and photochemical phenomena.[135,139,214,246,247,290–293] The linear vibronic coupling model (LVCM) is the simplest but effective

**FIGURE 7** Illustration of three Tully models and simulation results. Panel (a1) denotes diabatic PESes $V_{11}(R)$ and $V_{22}(R)$, as well as coupling term $V_{12}(R)$ for the SAC model; panel (b1) does so for the DAC model; panel (c1) does so for the ECR model. Panel (c2) demonstrates adiabatic PESes $E_1(R)$ and $E_2(R)$, as well as nonadiabatic coupling vector $d_{12}(R)$. Panels (a2–a3): transmission coefficients on diabatic state 1, and those on diabatic state 2 of the SAC model, respectively. Panels (b2–b3): similar to Panels (a2–a3), but for the DAC model. Panels (c3) and (c4): transmission/reflection coefficients on adiabatic state 1 of the ECR model; Panels (c5) and (c6): those on adiabatic state 2. In Panels (a2–a3), (b2–b3), and (c3–c6), magenta, purple, and green lines stand for transmission coefficients results for CMM with $\gamma = 0.366$, wMM with $\Delta = 0.1$, and wMM with $\Delta = 0.05$, respectively. Long-dashed blue lines: Ehrenfest dynamics; Short-dashed orange lines: FSSH; Black points: exact DVR benchmarks.

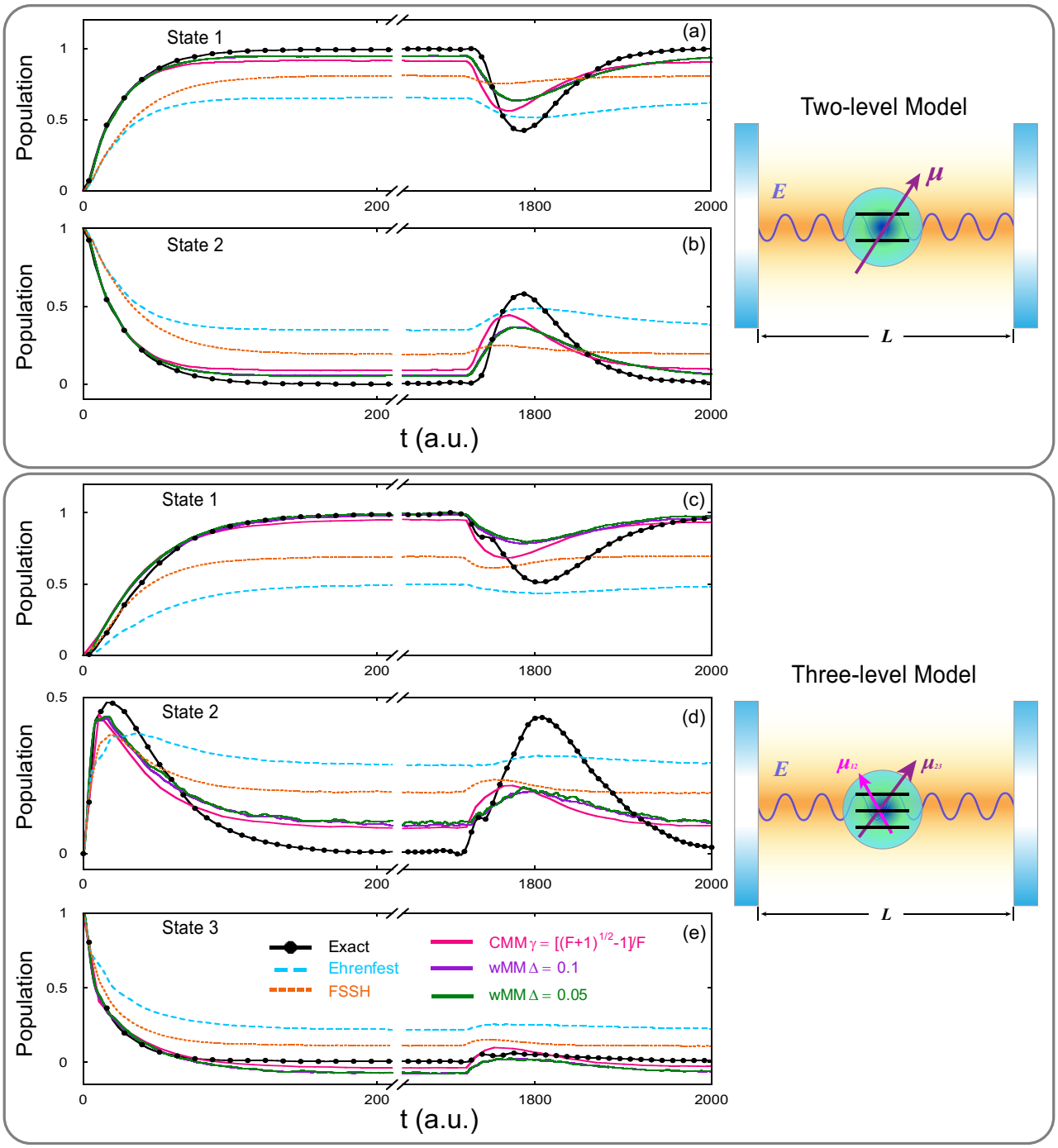


**FIGURE 8** Results of population dynamics for the atom-in-cavity models. Panels (a) and (b) represent data of the first and second states of the two-level model, respectively. Panels (c–e) denote data of the first, second, and third states of the three-level model, respectively. Magenta solid lines: CMM with $\gamma = \left(\sqrt{F+1}-1\right)/F$; purple solid lines: wMM with $\Delta = 0.1$; green solid lines: wMM with $\Delta = 0.05$; cyan long-dashed lines: Ehrenfest dynamics; Orange short-dashed lines: FSSH; black solid-dotted lines: Exact results from References 287,288. In each model, 400 continuous DOFs (i.e., standing-wave modes) are involved.

model widely used to describe dynamic properties around the conical intersection region, of which Hamiltonian in the diabatic representation is

$$\widehat{H} = \widehat{H}_0 + \widehat{H}_l + \widehat{H}_c. \tag{85}$$

Here, $\widehat{H}_0=\sum_{k=1}^{N}\omega_k\left(\widehat{P}_k^2+\widehat{R}_k^2\right)/2$ is the zeroth-order harmonic oscillator Hamiltonian in normal-mode space of the electronic ground state, where $\widehat{P}_k,\widehat{R}_k(k=1,...,N)$ denote the $k$-th effective weighted normal-mode variables with frequency $\omega_k$(i.e., $P_k=p_k/\sqrt{\omega_k}$, $R_k=\sqrt{\omega_k}r_k$, where $p_k,r_k$ are the canonical momentum, and canonical coordinate of $k$-th normal-mode). In Equation (85), $\widehat{H}_l=\sum_{n=1}^{F}\left(E_n+\sum_{k=1}^{N}\kappa_k^{(n)}\widehat{R}_k\right)|n\rangle\langle n|$ contains the vertical excitation energy, $E_n(n=1,...,F)$ of $F$ electronic states, and the linear coupling term $\kappa_k^{(n)}$ of each nuclear DOF for diagonal Hamiltonian elements, while $\widehat{H}_c=\sum_{n\neq m}^{F}\left(\sum_{k=1}^{N}\lambda_k^{(nm)}\widehat{R}_k\right)|n\rangle\langle m|$ includes linear coupling $\lambda_k^{(nm)}$ for each normal-mode between two different electronic states, $|n\rangle$ and $|m\rangle$.

A typical two-level 3-mode LVCM describes the S1/S2 conical intersection of the pyrazine molecule. The parameters of this model are fitted from semi-empirical electronic structure calculations by Schneiders and Domcke in Reference 294 The excitation energies for the two electronic states are $E_1=3.94$ eV and $E_2=4.84$ eV. The diagonal linear coupling terms of the first two modes $\{\widehat{R}_1,\widehat{R}_2\}$ are $\kappa_1^{(1)}=0.037$ eV, $\kappa_2^{(1)}=-0.105$ eV for the first electronic state, and $\kappa_1^{(2)}=-0.254$ eV, $\kappa_2^{(2)}=0.149$ eV for the second electronic state, respectively. The off-diagonal linear coupling of third mode $\widehat{R}_3$ is $\lambda_3^{(12)}=\lambda_3^{(21)}=0.262$ eV. The normal-mode vibronic frequency of each mode is $\omega_1=0.126$ eV, $\omega_2=0.074$ eV, and $\omega_3=0.118$ eV, respectively. Initial conditions of nuclear DOFs are sampled from the corresponding Wigner function of the vibronic ground state while the second electronic state is occupied. All simulations employ $\sim 10^5$ trajectories and time stepsize $\Delta t=0.01$ fs for fully converged results. Numerically exact result of this model calculated by ML-MCTDH are available in Reference [212].

Figure 9 shows population dynamics of state 2 yielded by wMM, CMM, Ehrenfest dynamics, FSSH and ML-MCTDH. It is evident that Ehrenfest dynamics performs poorly even for the short-time behavior (before 100 fs). In comparison, wMM, CMM, and FSSH more reasonably describe the radiationless energy transfer process at short time. Interestingly, wMM describes the oscillating behaviors in the long-time region (after 300 fs) better than other approximate methods. Such oscillating behavior in population dynamics indicates the molecular system passes through the "slopped" conical intersection region.[294]

Figures 6–9 demonstrate that the overall performance of wMM is better than CMM, especially in the gas phase scattering case of Figure 7c and the quantum electrodynamic light-matter systems of Figure 8. Both wMM and CMM approaches are able to outperform Ehrenfest dynamics as well as FSSH for condensed phase systems (e.g., in Figures 6 and 8).

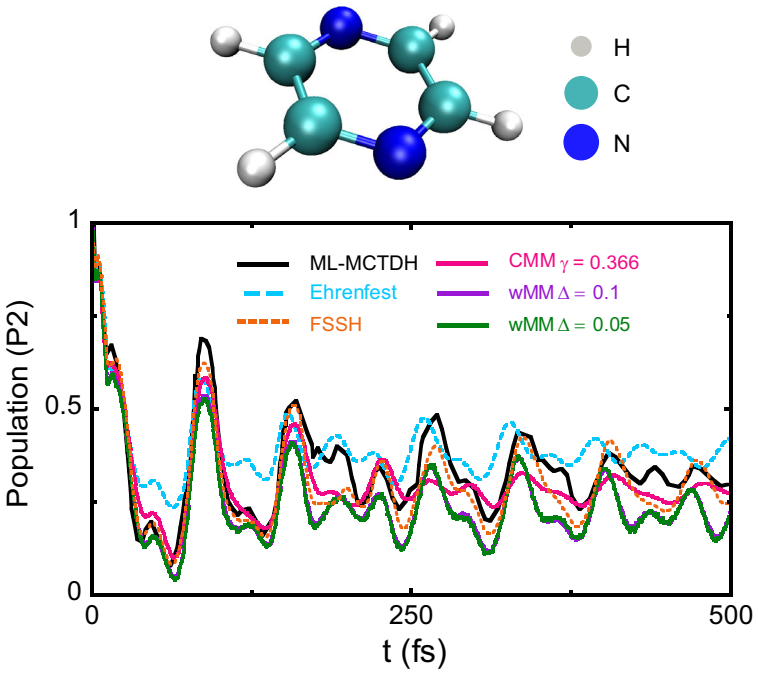


**FIGURE 9** Results of population dynamics of the second electronic state of the 2-level 3-mode pyrazine model. Magenta solid lines: CMM with $\gamma=\left(\sqrt{F+1}-1\right)/F\approx 0.366$; purple solid lines: wMM with $\Delta=0.1$; green solid lines: wMM with $\Delta=0.05$. Cyan dashed lines: Ehrenfest dynamics; Orange short-dashed lines: FSSH; black solid lines: ML-MCTDH results of Reference 212.

## 5 | CONCLUSION REMARKS

The phase space formulation of quantum mechanics not only presents a type of convenient interpretation to describe quantum-classical correspondences as well as nonclassical correlations/entanglement, but also sets the insightful scene for developing practical and useful trajectory-based quantum dynamics approaches.

In the Focus Article, we show that the constraint coordinate-momentum phase space formulation for the discrete-variable system which we have recently developed, and the weighted representation that we propose in the Focus Article are useful approaches for illustration of nonclassical features of quantum systems. The novel formulation is expected to have potential use for the illustration of nonclassical features of quantum states, as well as for future phase point measurement experiment.[70,85,221–234]

It is straightforward to show the relationship between the SU(F)/U(F-1) Stratonovich phase space[114] and constraint coordinate-momentum phase space, which is diffeomorphic to U(F)/U(F-1). When $F > 2$, it is inevitable to meet singularities in dynamics for discrete-variable systems when Stratonovich phase space is used (based on the symplectic structure of the phase space).[303] In comparison, (weighted) constraint coordinate-momentum phase space does not cause any singularities in trajectory-based exact dynamics, which is much more numerically favorable. (See more discussion in Appendix 3 of the Supporting Information).

When the general Moyal bracket of the quantum Liouville theorem is approximated by the corresponding Poisson bracket[57,58] on (weighted) constraint phase space, it reproduces the correct frozen-nuclei limit of composite/nonadiabatic systems. Such trajectory-based EOMs on (weighted) constraint coordinate-momentum phase space does not rely on the choice of representation of electronic states and are straightforward to obtain the form under covariant transformations. Because second-order nonadiabatic coupling terms are avoided in the EOMs of the adiabatic representation, it is especially useful for applications to realistic molecular systems. (In addition to Section 4.1, more discussion on the EOMs is presented in Appendices 2 and 5 of the Supporting Information.) Various benchmark model tests from gas phase to condensed phase quantum systems (as shown in Figures 6–9) indicate that wMM, the new trajectory-based approximate approach with the weighted constraint coordinate-momentum phase space representation, demonstrates overall better performance than FSSH as well as Ehrenfest dynamics. It is expected that more investigations on the (weighted) constraint phase space formulation will shed light on more numerically favorable dynamics approaches with the Meyer–Miller mapping Hamiltonian or other mapping Hamiltonians (e.g., those of Reference 131 and discussed in Reference 58).

We note that the (weighted) constraint coordinate-momentum phase space formulation is established for any systems with a finite set of states, not only limited to discrete electronic states, but also for finite discrete nuclear states. The weighted phase space strategy that we propose can also be applied to other types of phase space formulations of the discrete-variable system, such as Stratonovich phase space, and Wootters phase space, albeit the general coordinate-momentum phase space formulation presented in the Focus Article will be more convenient, for experimental measurements, tomography, or characterizations of fidelity, coherence, inequalities, displaced parity, atomic/molecular/optical Schrodinger cat states, and entanglement in quantum information and computation[70,85,221–234,295,296] as well as for studying dynamic processes of composite systems in physics, chemistry, materials, biology, and environmental science.

## AUTHOR CONTRIBUTIONS

**Xin He:** Conceptualization (equal); data curation (equal); formal analysis (equal); investigation (equal); methodology (equal); validation (equal); visualization (equal); writing – original draft (equal). **Baihua Wu:** Conceptualization (equal); data curation (equal); formal analysis (equal); investigation (equal); methodology (equal); validation (equal); visualization (equal); writing – original draft (equal). **Youhao Shang:** Conceptualization (supporting); formal analysis (supporting); investigation (supporting); methodology (supporting); validation (supporting); writing – original draft (supporting). **Bingqi Li:** Conceptualization (supporting); data curation (supporting); formal analysis (supporting); investigation (supporting); methodology (supporting); validation (supporting); visualization (supporting); writing – original draft (supporting). **Xiangsong Cheng:** Conceptualization (supporting); data curation (supporting); formal analysis (supporting); investigation (supporting); methodology (supporting); validation (supporting); visualization (supporting); writing – original draft (supporting). **Jian Liu:** Conceptualization (lead); data curation (lead); formal analysis (lead); funding acquisition (lead); investigation (lead); methodology (lead); project administration (lead); resources (lead); software (lead); supervision (lead); validation (lead); visualization (lead); writing – original draft (lead); writing – review and editing (lead).

## ACKNOWLEDGMENTS

This work was supported by the National Natural Science Foundation of China (NSFC) Grant No. 21961142017, and by the Ministry of Science and Technology of China (MOST) Grant No. 2017YFA0204901. We acknowledge the High-

performance Computing Platform of Peking University, Beijing PARATERA Tech CO., Ltd., and Guangzhou supercomputer center for providing computational resources.

## CONFLICT OF INTEREST

The authors have declared no conflicts of interest for this article.

## DATA AVAILABILITY STATEMENT

Data sharing is not applicable to this article as no new data were created or analyzed in this study.

## RESEARCH RESOURCES

High-performance Computing Platform of Peking University, Beijing PARATERA Tech CO., Ltd., and Guangzhou supercomputer center.

## ORCID

*Xin He* https://orcid.org/0000-0002-5189-7204
*Baihua Wu* https://orcid.org/0000-0002-1256-6859
*Youhao Shang* https://orcid.org/0000-0002-9297-6654
*Bingqi Li* https://orcid.org/0000-0001-7273-8299
*Xiangsong Cheng* https://orcid.org/0000-0001-8793-5092
*Jian Liu* https://orcid.org/0000-0002-2906-5858

## RELATED WIREs ARTICLES

Nonadiabatic dynamics: The SHARC approach
The hierarchical and perturbative forms of stochastic Schrodinger equations and their applications to carrier dynamics in organic materials

## REFERENCES

1. Lee HW, Scully MO. A new approach to molecular collisions: statistical quasiclassical method. J Chem Phys. 1980;73:2238–42. https://doi.org/10.1063/1.440419
2. Lee HW, Scully MO. The Wigner phase-space description of collision processes. Found Phys. 1983;13:61–72. https://doi.org/10.1007/bf01889411
3. Heller EJ. Wigner phase space method: analysis for semiclassical applications. J Chem Phys. 1976;65:1289–98. https://doi.org/10.1063/1.433238
4. Sun X, Wang H, Miller WH. Semiclassical theory of electronically nonadiabatic dynamics: results of a linearized approximation to the initial value representation. J Chem Phys. 1998;109:7064–74. https://doi.org/10.1063/1.477389
5. Wang H, Sun X, Miller WH. Semiclassical approximations for the calculation of thermal rate constants for chemical reactions in complex molecular systems. J Chem Phys. 1998;108:9726–36. https://doi.org/10.1063/1.476447
6. Pollak E, Liao J-L. A new quantum transition state theory. J Chem Phys. 1998;108:2733–43. https://doi.org/10.1063/1.475665
7. Shao J, Liao J-L, Pollak E. Quantum transition state theory: perturbation expansion. J Chem Phys. 1998;108:9711–25. https://doi.org/10.1063/1.476446
8. Hernandez R, Voth GA. Quantum time correlation functions and classical coherence. Chem Phys. 1998;233:243–55. https://doi.org/10.1016/s0301-0104(98)00027-5
9. Liu J, Miller WH. Using the thermal Gaussian approximation for the Boltzmann operator in semiclassical initial value time correlation functions. J Chem Phys. 2006;125:224104. https://doi.org/10.1063/1.2395941
10. Liu J, Miller WH. Linearized semiclassical initial value time correlation functions using the thermal Gaussian approximation: applications to condensed phase systems. J Chem Phys. 2007;127:114506. https://doi.org/10.1063/1.2774990
11. Liu J, Miller WH. Real time correlation function in a single phase space integral beyond the linearized semiclassical initial value representation. J Chem Phys. 2007;126:234110. https://doi.org/10.1063/1.2743023
12. Liu J, Miller WH. Linearized semiclassical initial value time correlation functions with maximum entropy analytic continuation. J Chem Phys. 2008;129:124111. https://doi.org/10.1063/1.2981065
13. Liu J, Miller WH. Test of the consistency of various linearized semiclassical initial value time correlation functions in application to inelastic neutron scattering from liquid para-hydrogen. J Chem Phys. 2008;128:144511. https://doi.org/10.1063/1.2889945
14. Liu J, Miller WH, Paesani F, Zhang W, Case DA. Quantum dynamical effects in liquid water: a semiclassical study on the diffusion and the infrared absorption spectrum. J Chem Phys. 2009;131:164509. https://doi.org/10.1063/1.3254372
15. Liu J, Miller WH. A simple model for the treatment of imaginary frequencies in chemical reaction rates and molecular liquids. J Chem Phys. 2009;131:074113. https://doi.org/10.1063/1.3202438

16. Liu J, Alder BJ, Miller WH. A semiclassical study of the thermal conductivity of low temperature liquids. J Chem Phys. 2011;135:114105. https://doi.org/10.1063/1.3639107
17. Liu J, Miller WH, Fanourgakis GS, Xantheas SS, Imoto S, Saito S. Insights in quantum dynamical effects in the infrared spectroscopy of liquid water from a semiclassical study with an ab initio-based flexible and polarizable force field. J Chem Phys. 2011;135:244503. https://doi.org/10.1063/1.3670960
18. Liu J. Recent advances in the linearized semiclassical initial value representation/classical Wigner model for the thermal correlation function. Int J Quantum Chem. 2015;115:657–70. https://doi.org/10.1002/qua.24872
19. Liu X, Liu J. Critical role of quantum dynamical effects in the Raman spectroscopy of liquid water. Mol Phys. 2018;116:755–79. https://doi.org/10.1080/00268976.2018.1434907
20. Shi Q, Geva E. Semiclassical theory of vibrational energy relaxation in the condensed phase. J Phys Chem A. 2003;107:9059–69. https://doi.org/10.1021/jp030497+
21. Shi Q, Geva E. A relationship between semiclassical and centroid correlation functions. J Chem Phys. 2003;118:8173–84. https://doi.org/10.1063/1.1564814
22. Ka BJ, Geva E. Vibrational energy relaxation of polyatomic molecules in liquid solution via the linearized semiclassical method. J Phys Chem A. 2006;110:9555–67. https://doi.org/10.1021/jp062363c
23. Poulsen JA, Nyman G, Rossky PJ. Practical evaluation of condensed phase quantum correlation functions: a Feynman-Kleinert variational linearized path integral method. J Chem Phys. 2003;119:12179–93. https://doi.org/10.1063/1.1626631
24. Poulsen JA, Nyman G, Rossky PJ. Feynman-Kleinert linearized path integral (FK-LPI) algorithms for quantum molecular dynamics, with application to water and He(4). J Chem Theory Comput. 2006;2:1482–91. https://doi.org/10.1021/ct600167s
25. Shao J, Makri N. Forward-backward semiclassical dynamics with linear scaling. J Phys Chem A. 1999;103:9479–86. https://doi.org/10.1021/jp991837n
26. Shao J, Makri N. Forward-backward semiclassical dynamics without prefactors. J Phys Chem A. 1999;103:7753–6. https://doi.org/10.1021/jp991433v
27. Liu J, Nakayama A, Makri N. Long-time behaviour of quantized distributions in forward–backward semiclassical dynamics. Mol Phys. 2006;104:1267–74. https://doi.org/10.1080/00268970500525754
28. Liu J, Makri N. Symmetries and detailed balance in forward–backward semiclassical dynamics. Chem Phys. 2006;322:23–9. https://doi.org/10.1016/j.chemphys.2005.08.010
29. Makri N, Nakayama A, Wright NJ. Forward-backward semiclassical simulation of dynamical properties in liquids. J Theor Comput Chem. 2004;3:391–417. https://doi.org/10.1142/s0219633604001112
30. Makri N. Quantum-classical path integral: a rigorous approach to condensed phase dynamics. Int J Quantum Chem. 2015;115:1209–14. https://doi.org/10.1002/qua.24975
31. Walters PL, Makri N. Quantum-classical path Integral simulation of ferrocene-ferrocenium charge transfer in liquid hexane. J Phys Chem Lett. 2015;6:4959–65. https://doi.org/10.1021/acs.jpclett.5b02265
32. Kryvohuz M, Cao JS. Quantum-classical correspondence in response theory. Phys Rev Lett. 2005;95:180405. https://doi.org/10.1103/PhysRevLett.95.180405
33. Donoso A, Martens CC. Quantum tunneling using entangled classical trajectories. Phys Rev Lett. 2001;87:223202. https://doi.org/10.1103/PhysRevLett.87.223202
34. Donoso A, Zheng Y, Martens CC. Simulation of quantum processes using entangled trajectory molecular dynamics. J Chem Phys. 2003;119:5010–20. https://doi.org/10.1063/1.1597496
35. Wang A, Zheng Y, Martens CC, Ren W. Quantum tunneling dynamics using entangled trajectories: general potentials. Phys Chem Chem Phys. 2009;11:1588–94. https://doi.org/10.1039/b811509e
36. Xu F, Martens CC, Zheng Y. Entanglement dynamics with a trajectory-based formulation. Phys Rev A. 2017;96:022138. https://doi.org/10.1103/PhysRevA.96.022138
37. Liu J, Miller WH. An approach for generating trajectory-based dynamics which conserves the canonical distribution in the phase space formulation of quantum mechanics. I Theories J Chem Phys. 2011;134:104101. https://doi.org/10.1063/1.3555273
38. Liu J, Miller WH. An approach for generating trajectory-based dynamics which conserves the canonical distribution in the phase space formulation of quantum mechanics. II. Thermal correlation functions. J Chem Phys. 2011;134:104102. https://doi.org/10.1063/1.3555274
39. Liu J. Two more approaches for generating trajectory-based dynamics which conserves the canonical distribution in the phase space formulation of quantum mechanics. J Chem Phys. 2011;134:194110. https://doi.org/10.1063/1.3589406
40. Liu J. Path integral Liouville dynamics for thermal equilibrium systems. J Chem Phys. 2014;140:224107. https://doi.org/10.1063/1.4881518
41. Liu J, Zhang Z. Path integral Liouville dynamics: applications to infrared spectra of OH, water, ammonia, and methane. J Chem Phys. 2016;144:034307. https://doi.org/10.1063/1.4939953
42. Liu J, Li D, Liu X. Further study of path integral Liouville dynamics. Sci Sin Chim. 2016;46:27–37. https://doi.org/10.1360/N032015-00143
43. Zhang Z, Chen Z, Liu J. Path integral Liouville dynamics simulations of vibrational spectra of formaldehyde and hydrogen peroxide. Chin J Chem Phys. 2020;33:613–22. https://doi.org/10.1063/1674-0068/cjcp2006099
44. Liu X, Zhang L, Liu J. Machine learning phase space quantum dynamics approaches. J Chem Phys. 2021;154:184104. https://doi.org/10.1063/5.0046689

45. Smith KKG, Poulsen JA, Nyman G, Cunsolo A, Rossky PJ. Application of a new ensemble conserving quantum dynamics simulation algorithm to liquid para-hydrogen and ortho-deuterium. J Chem Phys. 2015;142:244113. https://doi.org/10.1063/1.4922888
46. Smith KKG, Poulsen JA, Nyman G, Rossky PJ. A new class of ensemble conserving algorithms for approximate quantum dynamics: theoretical formulation and model problems. J Chem Phys. 2015;142:244112. https://doi.org/10.1063/1.4922887
47. Willatt MJ, Ceriotti M, Althorpe SC. Approximating Matsubara dynamics using the planetary model: tests on liquid water and ice. J Chem Phys. 2018;148:102336. https://doi.org/10.1063/1.5004808
48. Orr L, de la Pena LH, Roy P-N. Formulation of state projected centroid molecular dynamics: microcanonical ensemble and connection to the Wigner distribution. J Chem Phys. 2017;146:214116. https://doi.org/10.1063/1.4984229
49. Bonella S, Montemayor D, Coker DF. Linearized path integral approach for calculating nonadiabatic time correlation functions. Proc Natl Acad Sci USA. 2005;102:6715–9. https://doi.org/10.1073/pnas.0408326102
50. Nassimi A, Bonella S, Kapral R. Analysis of the quantum-classical Liouville equation in the mapping basis. J Chem Phys. 2010;133:134115. https://doi.org/10.1063/1.3480018
51. Weinbub J, Ferry DK. Recent advances in Wigner function approaches. Appl Phys Rev. 2018;5:041104. https://doi.org/10.1063/1.5046663
52. Pie T, Huppert S, Finocchi F, Depondt P, Bonella S. Sampling the thermal Wigner density via a generalized Langevin dynamics. J Chem Phys. 2019;151:114114. https://doi.org/10.1063/1.5099246
53. Kapral R, Ciccotti G. Mixed quantum-classical dynamics. J Chem Phys. 1999;110:8919–29. https://doi.org/10.1063/1.478811
54. Kapral R. Quantum dynamics in open quantum-classical systems. J Phys Condens Matter. 2015;27:073201. https://doi.org/10.1088/0953-8984/27/7/073201
55. Bai S, Xie W, Zhu L, Shi Q. Calculation of absorption spectra involving multiple excited states: approximate methods based on the mixed quantum classical Liouville equation. J Chem Phys. 2014;140:084105. https://doi.org/10.1063/1.4866367
56. Tao G, Miller WH. Semiclassical description of electronic excitation population transfer in a model photosynthetic system. J Phys Chem Lett. 2010;1:891–4. https://doi.org/10.1021/jz1000825
57. He X, Wu B, Gong Z, Liu J. Commutator matrix in phase space mapping models for nonadiabatic quantum dynamics. J Phys Chem A. 2021;125:6845–63. https://doi.org/10.1021/acs.jpca.1c04429
58. Liu J, He X, Wu B. Unified formulation of phase space mapping approaches for nonadiabatic quantum dynamics. Acc Chem Res. 2021;54:4215–28. https://doi.org/10.1021/acs.accounts.1c00511
59. Orioli AP, Safavi-Naini A, Wall ML, Rey AM. Nonequilibrium dynamics of spin-boson models from phase-space methods. Phys Rev A. 2017;96:033607. https://doi.org/10.1103/PhysRevA.96.033607
60. Lang H, Vendrell O, Hauke P. Generalized discrete truncated Wigner approximation for nonadiabatic quantum-classical dynamics. J Chem Phys. 2021;155:024111. https://doi.org/10.1063/5.0054696
61. Glauber RJ. Coherent and incoherent states of radiation field. Phys Rev. 1963;131:2766. https://doi.org/10.1103/PhysRev.131.2766
62. Sudarshan ECG. Equivalence of semiclassical and quantum mechanical descriptions of statistical light beams. Phys Rev Lett. 1963;10:277. https://doi.org/10.1103/PhysRevLett.10.277
63. Cahill KE, Glauber RJ. Ordered expansions in boson amplitude operators. Phys Rev. 1969;177:1857. https://doi.org/10.1103/PhysRev.177.1857
64. Cahill KE, Glauber RJ. Density operators and quasiprobability distributions. Phys Rev. 1969;177:1882. https://doi.org/10.1103/PhysRev.177.1882
65. Arecchi FT, Courtens E, Gilmore R, Thomas H. Atomic coherent states in quantum optics. Phys Rev A. 1972;6:2211. https://doi.org/10.1103/PhysRevA.6.2211
66. Drummond PD, Gardiner CW. Generalized P-representations in quantum optics. J Phys A Math Gen. 1980;13:2353–68. https://doi.org/10.1088/0305-4470/13/7/018
67. Walls DF, Millburm GJ. Quantum Optics. Berlin: Springer-Verlag; 1994.
68. Gardiner C, Zoller P. Quantum Noise: A Handbook of Markovian and Non-Markovian Quantum Stochastic Methods with Applications to Quantum Optics. 3rd ed. Berlin Heidelberg: Springer-Verlag; 2004.
69. Schleich WP. Quantum Optics in Phase Space. Berlin: Wiley-VCH Verlag Berlim GmbH; 2001.
70. Deléglise S, Dotsenko I, Sayrin C, Bernu J, Brune M, Raimond J-M, et al. Reconstruction of non-classical cavity field states with snapshots of their decoherence. Nature. 2008;455:510–4. https://doi.org/10.1038/nature07288
71. Steel MJ, Olsen MK, Plimak LI, Drummond PD, Tan SM, Collett MJ, et al. Dynamical quantum noise in trapped Bose-Einstein condensates. Phys Rev A. 1998;58:4824–35. https://doi.org/10.1103/PhysRevA.58.4824
72. Sinatra A, Lobo C, Castin Y. The truncated Wigner method for Bose-condensed gases: limits of validity and applications. J Phys B Atomic Mol Opt Phys. 2002;35:3599–631. https://doi.org/10.1088/0953-4075/35/17/301
73. Blakie PB, Bradley AS, Davis MJ, Ballagh RJ, Gardiner CW. Dynamics and statistical mechanics of ultra-cold Bose gases using c-field techniques. Adv Phys. 2008;57:363–455. https://doi.org/10.1080/00018730802564254
74. Polkovnikov A. Phase space representation of quantum dynamics. Ann Phys. 2010;325:1790–852. https://doi.org/10.1016/j.aop.2010.02.006
75. Mukherjee R, Mirasola AE, Hollingsworth J, White IG, Hazzard KRA. Geometric representation of spin correlations and applications to ultracold systems. Phys Rev A. 2018;97:043606. https://doi.org/10.1103/physreva.97.043606
76. Zurek WH. Sub-Planck structure in phase space and its relevance for quantum decoherence. Nature. 2001;412:712–7. https://doi.org/10.1038/35089017

77. Miquel C, Paz JP, Saraceno M. Quantum computers in phase space. Phys Rev A. 2002;65:062309. https://doi.org/10.1103/PhysRevA.65.062309
78. Wootters WK. Picturing qubits in phase space. IBM J Res Dev. 2004;48:99–110. https://doi.org/10.1147/rd.481.0099
79. Paz JP, Roncaglia AJ, Saraceno M. Qubits in phase space: Wigner-function approach to quantum-error correction and the mean-king problem. Phys Rev A. 2005;72:012309. https://doi.org/10.1103/PhysRevA.72.012309
80. Braunstein SL, van Loock P. Quantum information with continuous variables. Rev Mod Phys. 2005;77:513–77. https://doi.org/10.1103/RevModPhys.77.513
81. Delfosse N, Guerin PA, Bian J, Raussendorf R. Wigner function negativity and contextuality in quantum computation on rebits. Phys Rev X. 2015;5:021003. https://doi.org/10.1103/PhysRevX.5.021003
82. Schachenmayer J, Pikovski A, Rey AM. Many-body quantum spin dynamics with Monte-Carlo trajectories on a discrete phase space. Phys Rev X. 2015;5:011022. https://doi.org/10.1103/PhysRevX.5.011022
83. Schachenmayer J, Pikovski A, Rey AM. Dynamics of correlations in two-dimensional quantum spin models with long-range interactions: a phase-space Monte-Carlo study. New J Phys. 2015;17:065009. https://doi.org/10.1088/1367-2630/17/6/065009
84. Bermejo-Vega J, Delfosse N, Browne DE, Okay C, Raussendorf R. Contextuality as a resource for models of quantum computation with qubits. Phys Rev Lett. 2017;119:120505. https://doi.org/10.1103/PhysRevLett.119.120505
85. Rundle RP, Mills PW, Tilma T, Samson JH, Everitt MJ. Simple procedure for phase-space measurement and entanglement validation. Phys Rev A. 2017;96:022117. https://doi.org/10.1103/physreva.96.022117
86. Zhu B, Rey AM, Schachenmayer J. A generalized phase space approach for solving quantum spin dynamics. New J Phys. 2019;21:082001. https://doi.org/10.1088/1367-2630/ab354d
87. Rundle RP, Everitt MJ. Overview of the phase space formulation of quantum mechanics with application to quantum technologies. Adv Quantum Technol. 2021;4:2100016. https://doi.org/10.1002/qute.202100016
88. Weyl H. Quantum mechanics and group theory. Z Phys. 1927;46:1–46. https://doi.org/10.1007/bf02055756
89. Wigner EP. On the quantum correction for thermodynamic equilibrium. Phys Rev. 1932;40:749–59. https://doi.org/10.1103/physrev.40.749
90. Hillery M, Oconnell RF, Scully MO, Wigner EP. Distribution-functions in physics: fundamentals. Phys Rep. 1984;106:121–67. https://doi.org/10.1016/0370-1573(84)90160-1
91. Lee HW. Theory and application of the quantum phase-space distribution functions. Phys Rep. 1995;259:147–211. https://doi.org/10.1016/0370-1573(95)00007-4
92. Cohen L. Generalized phase-space distribution functions. J Math Phys. 1966;7:781–6. https://doi.org/10.1063/1.1931206
93. Groenewold HJ. On the Principles of Elementary Quantum Mechanics. Phys Ther. 1946;12:405–60. https://doi.org/10.1016/s0031-8914(46)80059-4
94. Moyal JE. Quantum mechanics as a statistical theory. Math Proc Cambridge Phil Soc. 1949;45:99–124. https://doi.org/10.1017/s0305004100000487
95. Bopp F. Werner Heisenberg und die Physik unserer Zeit. Wiesbaden: Vieweg+Teubner Verlag; 1961.
96. Miller WH. Quantum dynamics of complex molecular systems. Proc Natl Acad Sci USA. 2005;102:6660–4. https://doi.org/10.1073/pnas.0408043102
97. Miller WH. Including quantum effects in the dynamics of complex (i.e., large) molecular systems. J Chem Phys 2006;125:132305. https://doi.org/10.1063/1.2211608
98. Miller WH. Classical-limit quantum mechanics and the theory of molecular collisions. Adv Chem Phys. 1974;25:69–177. https://doi.org/10.1002/9780470143773.ch2
99. Miller WH. The classical S-matrix in molecular collisions. Adv Chem Phys. 1975;30:77. https://doi.org/10.1002/9780470143827.ch3
100. Stratonovich RL. On distributions in represenation space. Zh Eksp Teor Fiz. 1956;31:1012.
101. Feynman RP. Negative probability. In: Hiley BJ, Peat D, editors. Quantum Implications: Essays in Honour of David Bohm. New York: Routledge; 1987. p. 235–48.
102. Wootters WK. A Wigner-function formulation of finite-state quantum mechanics. Ann Phys. 1987;176:1–21. https://doi.org/10.1016/0003-4916(87)90176-x
103. Várilly JC, Gracia-Bonda J. The Moyal representation for spin. Ann Phys. 1989;190:107–48. https://doi.org/10.1016/0003-4916(89)90262-5
104. Amiet JP, Cibils MB. Description of quantum spin using functions on the sphere $S^2$. J Phys A Math Gen. 1991;24:1515–35. https://doi.org/10.1088/0305-4470/24/7/023
105. Amiet JP, Weigert S. Discrete Q- and P-symbols for spin s. J Opt B Quantum Semiclassical Opt. 2000;2:118–21. https://doi.org/10.1088/1464-4266/2/2/309
106. Dowling JP, Agarwal GS, Schleich WP. Wigner distribution of a general angular-momentum state: applications to a collection of 2-level atoms. Phys Rev A. 1994;49:4101–9. https://doi.org/10.1103/PhysRevA.49.4101
107. Brif C, Mann A. Phase-space formulation of quantum mechanics and quantum-state reconstruction for physical systems with Lie-group symmetries. Phys Rev A. 1999;59:971–87. https://doi.org/10.1103/physreva.59.971
108. Cunha MOT, Man'ko VI, Scully MO. Quasiprobability and probability distributions for spin-1/2 states. Found Phys Lett. 2001;14:103–17. https://doi.org/10.1023/a:1012373419313
109. Klimov AB, Espinoza P. Moyal-like form of the star product for generalized SU(2) Stratonovich-Weyl symbols. J Phys A Math Gen. 2002;35:8435–47. https://doi.org/10.1088/0305-4470/35/40/305

110. Klimov AB, Romero JL. A generalized Wigner function for quantum systems with the SU(2) dynamical symmetry group. J Phys A Math Theor. 2008;41:055303. https://doi.org/10.1088/1751-8113/41/5/055303
111. Klimov AB, Romero JL, de Guise H. Generalized SU(2) covariant Wigner functions and some of their applications. J Phys A Math Theor. 2017;50:323001. https://doi.org/10.1088/1751-8121/50/32/323001
112. Adam P, Andreev VA, Man'ko MA, Man'ko VI, Mechler M. SU(2) symmetry of qubit states and Heisenberg-Weyl symmetry of systems with continuous variables in the probability representation of quantum mechanics. Symmetry. 2020;12:23. https://doi.org/10.3390/sym12071099
113. Koczor B, Zeier R, Glaser SJ. Continuous phase-space representations for finite-dimensional quantum states and their tomography. Phys Rev A. 2020;101:022318. https://doi.org/10.1103/physreva.101.022318
114. Tilma T, Nemoto K. SU(N)-symmetric quasi-probability distribution functions. J Phys A Math Theor. 2012;45:015302. https://doi.org/10.1088/1751-8113/45/1/015302
115. Tilma T, Everitt MJ, Samson JH, Munro WJ, Nemoto K. Wigner functions for arbitrary quantum systems. Phys Rev Lett. 2016;117:180401. https://doi.org/10.1103/physrevlett.117.180401
116. Marchiolli MA, Galetti D. On the discrete Wigner function for SU(N). J Phys A Math Theor. 2019;52:405305. https://doi.org/10.1088/1751-8121/ab3bab
117. Rundle RP, Tilma T, Samson JH, Dwyer VM, Bishop RF, Everitt MJ. General approach to quantum mechanics as a statistical theory. Phys Rev A. 2019;99:012115. https://doi.org/10.1103/physreva.99.012115
118. Cohendet O, Combe P, Sirugue M, Sirugue-Collin M. A stochastic treatment of the dynamics of an integer spin. J Phys A Math Gen. 1988;21:2875–83. https://doi.org/10.1088/0305-4470/21/13/012
119. Leonhardt U. Quantum-state tomography and discrete Wigner function. Phys Rev Lett. 1995;74:4101–5. https://doi.org/10.1103/PhysRevLett.74.4101
120. Leonhardt U. Discrete Wigner function and quantum-state tomography. Phys Rev A. 1996;53:2998–3013. https://doi.org/10.1103/PhysRevA.53.2998
121. Gibbons KS, Hoffman MJ, Wootters WK. Discrete phase space based on finite fields. Phys Rev A. 2004;70:062101. https://doi.org/10.1103/physreva.70.062101
122. Wootters WK. Quantum measurements and finite geometry. Found Phys. 2006;36:112–26. https://doi.org/10.1007/s10701-005-9008-x
123. Ruzzi M, Marchiolli MA, Galetti D. Extended Cahill-Glauber formalism for finite-dimensional spaces: I. Fundamentals. J Phys A Math Gen. 2005;38:6239–51. https://doi.org/10.1088/0305-4470/38/27/010
124. Chaturvedi S, Ercolessi E, Marmo G, Morandi G, Mukunda N, Simon R. Wigner distributions for finite dimensional quantum systems: an algebraic approach. Pramana. 2005;65:981–93. https://doi.org/10.1007/bf02705275
125. Chaturvedi S, Ercolessi E, Marmo G, Morandi G, Mukunda N, Simon R. Wigner-Weyl correspondence in quantum mechanics for continuous and discrete systems-a Dirac-inspired view. J Phys A Math Gen. 2006;39:1405–23. https://doi.org/10.1088/0305-4470/39/6/014
126. Gross D. Hudson's theorem for finite-dimensional quantum systems. J Math Phys. 2006;47:25. https://doi.org/10.1063/1.2393152
127. Valtierra IF, Romero JL, Klimov AB. TWA versus semiclassical unitary approximation for spin-like systems. Ann Phys. 2017;383:620–34. https://doi.org/10.1016/j.aop.2017.06.006
128. Valtierra IF, Klimov AB, Leuchs G, Sánchez-Soto LL. Quasiprobability currents on the sphere. Phys Rev A. 2020;101:033803. https://doi.org/10.1103/PhysRevA.101.033803
129. Czischek S. Discrete Truncated Wigner Approximation. Neural-Network Simulation of Strongly Correlated Quantum Systems. Cham: Springer; 2020. p. 85–109. https://doi.org/10.1007/978-3-030-52715-0_4
130. Morales-Hernández GE, Castellanos JC, Romero JL, Klimov AB. Semi-classical discretization and long-time evolution of variable spin systems. Entropy. 2021;23:684. https://doi.org/10.3390/e23060684
131. Liu J. A unified theoretical framework for mapping models for the multi-state Hamiltonian. J Chem Phys. 2016;145:204105. https://doi.org/10.1063/1.4967815
132. He X, Liu J. A new perspective for nonadiabatic dynamics with phase space mapping models. J Chem Phys. 2019;151:024105. https://doi.org/10.1063/1.5108736
133. Liu J. Isomorphism between the multi-state Hamiltonian and the second-quantized many-electron Hamiltonian with only 1-electron interactions. J Chem Phys. 2017;146:024110. https://doi.org/10.1063/1.4973708
134. He X, Gong Z, Wu B, Liu J. Negative zero-point-energy parameter in the Meyer-Miller mapping model for nonadiabatic dynamics. J Phys Chem Lett. 2021;12:2496–501. https://doi.org/10.1021/acs.jpclett.1c00232
135. Domcke W, Yarkony DR, Köppel H. Conical Intersections: Theory, Computation and Experiment. Singapore: World Scientific; 2011. https://doi.org/10.1142/7803
136. Yonehara T, Hanasaki K, Takatsuka K. Fundamental approaches to nonadiabaticity: toward a chemical theory beyond the Born-Oppenheimer paradigm. Chem Rev. 2011;112:499–542. https://doi.org/10.1021/cr200096s
137. Tully JC. Perspective: nonadiabatic dynamics theory. J Chem Phys. 2012;137:22A301. https://doi.org/10.1063/1.4757762
138. Miller WH, Cotton SJ. Classical molecular dynamics simulation of electronically non-adiabatic processes. Faraday Discuss. 2016;195:9–30. https://doi.org/10.1039/c6fd00181e
139. Levine BG, Martínez TJ. Isomerization through conical intersections. Annu Rev Phys Chem. 2007;58:613–34. https://doi.org/10.1146/annurev.physchem.57.032905.104612
140. Martínez TJ. Seaming is believing. Nature. 2010;467:412–3. https://doi.org/10.1038/467412a

141. Sisto A, Glowacki DR, Martínez TJ. Ab Initio nonadiabatic dynamics of multichromophore complexes: a scalable graphical-processing-unit-accelerated exciton framework. Acc Chem Res. 2014;47:2857–66. https://doi.org/10.1021/ar500229p
142. Makhov DV, Glover WJ, Martínez TJ, Shalashilin DV. Ab initio multiple cloning algorithm for quantum nonadiabatic molecular dynamics. J Chem Phys. 2014;141:054110. https://doi.org/10.1063/1.4891530
143. Mai S, Marquetand P, González L. Nonadiabatic dynamics: the SHARC approach. WIREs Comput Mol Sci. 2018;8:e1370. https://doi.org/10.1002/wcms.1370
144. Mai S, González L. Molecular photochemistry: recent developments in theory. Angew Chem Int Ed. 2020;59:16832–46. https://doi.org/10.1002/anie.201916381
145. Subotnik JE, Jain A, Landry B, Petit A, Ouyang W, Bellonzi N. Understanding the surface hopping view of electronic transitions and decoherence. Annu Rev Phys Chem. 2016;67:387–417. https://doi.org/10.1146/annurev-physchem-040215-112245
146. Fang W-H. Ab Initio determination of dark structures in radiationless transitions for aromatic carbonyl compounds. Acc Chem Res. 2008;41:452–7. https://doi.org/10.1021/ar700205f
147. Long R, Prezhdo OV, Fang W-H. Nonadiabatic charge dynamics in novel solar cell materials. WIREs Comput Mol Sci. 2017;7:e1305. https://doi.org/10.1002/wcms.1305
148. Feng W, Xu L, Li X-Q, Fang W-H, Yan Y. Nonadiabatic molecular dynamics simulation: an approach based on quantum measurement picture. AIP Adv. 2014;4:077131. https://doi.org/10.1063/1.4891821
149. Lan Z, Shao J. Approximate theoretical methods for nonadiabatic dynamics of polyatomic molecules. Prog Chem. 2012;24:1105–19.
150. Wang Y-C, Ke Y, Zhao Y. The hierarchical and perturbative forms of stochastic Schrodinger equations and their applications to carrier dynamics in organic materials. WIREs Comput Mol Sci. 2019;9:e1375. https://doi.org/10.1002/wcms.1375
151. Nelson T, Fernandez-Alberti S, Roitberg AE, Tretiak S. Nonadiabatic excited-state molecular dynamics: modeling photophysics in organic conjugated materials. Acc Chem Res. 2014;47:1155–64. https://doi.org/10.1021/ar400263p
152. Crespo-Otero R, Barbatti M. Recent advances and perspectives on nonadiabatic mixed quantum-classical dynamics. Chem Rev. 2018;118:7026–68. https://doi.org/10.1021/acs.chemrev.7b00577
153. Meyer H-D, Miller WH. A classical analog for electronic degrees of freedom in nonadiabatic collision processes. J Chem Phys. 1979;70:3214–23. https://doi.org/10.1063/1.437910
154. Stock G, Thoss M. Semiclassical description of nonadiabatic quantum dynamics. Phys Rev Lett. 1997;78:578–81. https://doi.org/10.1103/PhysRevLett.78.578
155. Wigner EP. Perspectives in Quantum Theory. Cambridge, MA: MIT Press; 1971.
156. Husimi K. Some formal properties of the density matrix. Proc Physico-Math Soc Jpn. 1940;22:264–314. https://doi.org/10.11429/ppmsj1919.22.4_264
157. Glauber RJ. Optical coherence and photon statistics. In: deWitt C, Blandin A, Cohen-Tannoudji C, editors. Quantum Optics and Electronics. New York: Gordon and Breach; 1965. pp. 23–182.
158. Kirkwood JG. Quantum statistics of almost classical assemblies. Phys Rev. 1933;44:31. https://doi.org/10.1103/PhysRev.44.31
159. Rihaczek A. Signal energy distribution in time and frequency. IEEE Trans Inform Theory. 1968;14:369–74. https://doi.org/10.1109/TIT.1968.1054157
160. Mehta CL. Phase-space formulation of the dynamics of canonical variables. J Math Phys. 1964;5:677–86. https://doi.org/10.1063/1.1704163
161. Rivier DC. On a one-to-one correspondence between infinitesimal canonical transformations and infinitesimal unitary transformations. Phys Rev. 1951;83:862. https://doi.org/10.1103/PhysRev.83.862
162. Margenau H, Hill RN. Correlation between measurements in quantum theory. Prog Theor Phys. 1961;26:722–38. https://doi.org/10.1143/PTP.26.722
163. Born M, Jordan P. On quantum mechanics. Z Phys. 1925;34:858–88. https://doi.org/10.1007/BF01328531
164. Meyer H-D, Miller WH. Classical-models for electronic degrees of freedom: derivation via spin analogy and application to $F^* + H_2 \rightarrow F + H_2$. J Chem Phys. 1979;71:2156–69. https://doi.org/10.1063/1.438598
165. Gray SK, Miller WH. Classical model for electronic degrees of freedom: charge transfer in Na + I collisions. Chem Phys Lett. 1982;93:341–4. https://doi.org/10.1016/0009-2614(82)83705-6
166. Ali DP, Miller WH. Effect of electronic transition dynamics on iodine atom recombination in liquids. J Chem Phys. 1983;78:6640–5. https://doi.org/10.1063/1.444662
167. Ali DP, Miller WH. Classical models for electronic degrees of freedom: quenching of Br*(2P1/2) by collision with $H_2$ in three dimensions. Chem Phys Lett. 1984;103:470–4. https://doi.org/10.1016/0009-2614(84)85279-3
168. Stock G, Miller WH. A classical model for time- and frequency-resolved spectroscopy of nonadiabatic excited-state dynamics. Chem Phys Lett. 1992;197:396–404. https://doi.org/10.1016/0009-2614(92)85791-8
169. Stock G, Miller WH. Classical formulation of the spectroscopy of nonadiabatic excited-state dynamics. J Chem Phys. 1993;99:1545–55. https://doi.org/10.1063/1.465323
170. Sun X, Miller WH. Semiclassical initial value representation for electronically nonadiabatic molecular dynamics. J Chem Phys. 1997;106:6346–53. https://doi.org/10.1063/1.473624
171. Coronado EA, Batista VS, Miller WH. Nonadiabatic photodissociation dynamics of ICN in the Ã continuum: a semiclassical initial value representation study. J Chem Phys. 2000;112:5566–75. https://doi.org/10.1063/1.481130
172. Coronado EA, Xing J, Miller WH. Ultrafast non-adiabatic dynamics of systems with multiple surface crossings: a test of the Meyer-Miller Hamiltonian with semiclassical initial value representation methods. Chem Phys Lett. 2001;349:521–9. https://doi.org/10.1016/s0009-2614(01)01242-8

173. Ananth N, Venkataraman C, Miller WH. Semiclassical description of electronically nonadiabatic dynamics via the initial value representation. J Chem Phys. 2007;127:084114. https://doi.org/10.1063/1.2759932
174. Miller WH. Electronically nonadiabatic dynamics via semiclassical initial value methods. J Phys Chem A. 2009;113:1405–15. https://doi.org/10.1021/jp809907p
175. Ananth N, Miller TF. Exact quantum statistics for electronically nonadiabatic systems using continuous path variables. J Chem Phys. 2010;133:234103. https://doi.org/10.1063/1.3511700
176. Cotton SJ, Miller WH. Symmetrical windowing for quantum states in quasi-classical trajectory simulations. J Phys Chem A. 2013;117:7190–4. https://doi.org/10.1021/jp401078u
177. Cotton SJ, Miller WH. Symmetrical windowing for quantum states in quasi-classical trajectory simulations: application to electronically non-adiabatic processes. J Chem Phys. 2013;139:234112. https://doi.org/10.1063/1.4845235
178. Cotton SJ, Igumenshchev K, Miller WH. Symmetrical windowing for quantum states in quasi-classical trajectory simulations: application to electron transfer. J Chem Phys. 2014;141:084104. https://doi.org/10.1063/1.4893345
179. Cotton SJ, Miller WH. A symmetrical quasi-classical spin-mapping model for the electronic degrees of freedom in non-adiabatic processes. J Phys Chem A. 2015;119:12138–45. https://doi.org/10.1021/acs.jpca.5b05906
180. Miller WH, Cotton SJ. Communication: note on detailed balance in symmetrical quasi-classical models for electronically non-adiabatic dynamics. J Chem Phys. 2015;142:131103. https://doi.org/10.1063/1.4916945
181. Cotton SJ, Miller WH. A new symmetrical quasi-classical model for electronically non-adiabatic processes: application to the case of weak non-adiabatic coupling. J Chem Phys. 2016;145:144108. https://doi.org/10.1063/1.4963914
182. Cotton SJ, Miller WH. The symmetrical quasi-classical model for electronically non-adiabatic processes applied to energy transfer dynamics in site-exciton models of light-harvesting complexes. J Chem Theory Comput. 2016;12:983–91. https://doi.org/10.1021/acs.jctc.5b01178
183. Miller WH, Cotton SJ. Communication: Wigner functions in action-angle variables, Bohr-Sommerfeld quantization, the Heisenberg correspondence principle, and a symmetrical quasi-classical approach to the full electronic density matrix. J Chem Phys. 2016;145:081102. https://doi.org/10.1063/1.4961551
184. Cotton SJ, Liang R, Miller WH. On the adiabatic representation of Meyer-Miller electronic-nuclear dynamics. J Chem Phys. 2017;147:064112. https://doi.org/10.1063/1.4995301
185. Liang R, Cotton SJ, Binder R, Hegger R, Burghardt I, Miller WH. The symmetrical quasi-classical approach to electronically nonadiabatic dynamics applied to ultrafast exciton migration processes in semiconducting polymers. J Chem Phys. 2018;149:044101. https://doi.org/10.1063/1.5037815
186. Cotton SJ, Miller WH. A symmetrical quasi-classical windowing model for the molecular dynamics treatment of non-adiabatic processes involving many electronic states. J Chem Phys. 2019;150:104101. https://doi.org/10.1063/1.5087160
187. Cotton SJ, Miller WH. Trajectory-adjusted electronic zero point energy in classical Meyer-Miller vibronic dynamics: symmetrical quasiclassical application to photodissociation. J Chem Phys. 2019;150:194110. https://doi.org/10.1063/1.5094458
188. Müller U, Stock G. Flow of zero-point energy and exploration of phase space in classical simulations of quantum relaxation dynamics. II. Application to nonadiabatic processes. J Chem Phys. 1999;111:77–88. https://doi.org/10.1063/1.479255
189. Stock G, Müller U. Flow of zero-point energy and exploration of phase space in classical simulations of quantum relaxation dynamics. J Chem Phys. 1999;111:65–76. https://doi.org/10.1063/1.479254
190. Müller U, Stock G. Consistent treatment of quantum-mechanical and classical degrees of freedom in mixed quantum-classical simulations. J Chem Phys. 1998;108:7516–26. https://doi.org/10.1063/1.476184
191. Stock G, Thoss M. Classical description of nonadiabatic quantum dynamics. Adv Chem Phys. 2005;131:243–375. https://doi.org/10.1002/0471739464.ch5
192. Thoss M, Miller WH, Stock G. Semiclassical description of nonadiabatic quantum dynamics: application to the S1-S2 conical intersection in pyrazine. J Chem Phys. 2000;112:10282–92. https://doi.org/10.1063/1.481668
193. Thoss M, Stock G. Mapping approach to the semiclassical description of nonadiabatic quantum dynamics. Phys Rev A. 1999;59:64–79. https://doi.org/10.1103/PhysRevA.59.64
194. Golosov AA, Reichman DR. Classical mapping approaches for nonadiabatic dynamics: short time analysis. J Chem Phys. 2001;114:1065–74. https://doi.org/10.1063/1.1332812
195. Saller MAC, Kelly A, Richardson JO. On the identity of the identity operator in nonadiabatic linearized semiclassical dynamics. J Chem Phys. 2019;150:071101. https://doi.org/10.1063/1.5082596
196. Saller MAC, Kelly A, Richardson JO. Improved population operators for multi-state nonadiabatic dynamics with the mixed quantum-classical mapping approach. Faraday Discuss. 2020;221:150–67. https://doi.org/10.1039/c9fd00050j
197. Runeson JE, Richardson JO. Generalized spin mapping for quantum-classical dynamics. J Chem Phys. 2020;152:084110. https://doi.org/10.1063/1.5143412
198. Kananenka AA, Hsieh CY, Cao JS, Geva E. Nonadiabatic dynamics via the symmetrical quasi-classical method in the presence of anharmonicity. J Phys Chem Lett. 2018;9:319–26. https://doi.org/10.1021/acs.jpclett.7b03002
199. Mulvihill E, Gao X, Liu Y, Schubert A, Dunietz BD, Geva E. Combining the mapping Hamiltonian linearized semiclassical approach with the generalized quantum master equation to simulate electronically nonadiabatic molecular dynamics. J Chem Phys. 2019;151:074103. https://doi.org/10.1063/1.5110891
200. Gao X, Geva E. Improving the accuracy of quasiclassical mapping Hamiltonian methods by treating the window function width as an adjustable parameter. J Phys Chem A. 2020;124:11006–16. https://doi.org/10.1021/acs.jpca.0c09750

201. Gao X, Lai Y, Geva E. Simulating absorption spectra of multiexcitonic systems via quasiclassical mapping Hamiltonian methods. J Chem Theory Comput. 2020;16:6465–80. https://doi.org/10.1021/acs.jctc.0c00709
202. Gao X, Sailer MAC, Liu Y, Kelly A, Richardson JO, Geva E. Benchmarking quasiclassical mapping Hamiltonian methods for simulating electronically nonadiabatic molecular dynamics. J Chem Theory Comput. 2020;16:2883–95. https://doi.org/10.1021/acs.jctc.9b01267
203. Liu Y, Gao X, Lai Y, Mulvihill E, Geva E. Electronic dynamics through conical intersections via quasiclassical mapping Hamiltonian methods. J Chem Theory Comput. 2020;16:4479–88. https://doi.org/10.1021/acs.jctc.0c00177
204. Saller MAC, Kelly A, Geva E. Benchmarking quasiclassical mapping Hamiltonian methods for simulating cavity-modified molecular dynamics. J Phys Chem Lett. 2021;12:3163–70. https://doi.org/10.1021/acs.jpclett.1c00158
205. Bonella S, Coker DF. A semiclassical limit for the mapping Hamiltonian approach to electronically nonadiabatic dynamics. J Chem Phys. 2001;114:7778–89. https://doi.org/10.1063/1.1366331
206. Bonella S, Coker DF. Semiclassical implementation of the mapping Hamiltonian approach for nonadiabatic dynamics using focused initial distribution sampling. J Chem Phys. 2003;118:4370–85. https://doi.org/10.1063/1.1542883
207. Bonella S, Coker DF. LAND-map, a linearized approach to nonadiabatic dynamics using the mapping formalism. J Chem Phys. 2005; 122:194102. https://doi.org/10.1063/1.1896948
208. Huo PF, Coker DF. Semi-classical path integral non-adiabatic dynamics: a partial linearized classical mapping Hamiltonian approach. Mol Phys. 2012;110:1035–52. https://doi.org/10.1080/00268976.2012.684896
209. Tang D, Fang W-H, Shen L, Cui G. Combining Meyer-Miller Hamiltonian with electronic structure methods for on-the-fly nonadiabatic dynamics simulations: implementation and application. Phys Chem Chem Phys. 2019;21:17109–17. https://doi.org/10.1039/c9cp02682g
210. Zheng J, Xie Y, Jiang S, Long Y, Ning X, Lan Z. Ultrafast electron transfer with symmetrical quasi-classical dynamics based on mapping Hamiltonian and quantum dynamics based on ML-MCTDH. Chin J Chem Phys. 2017;30:800–10. https://doi.org/10.1063/1674-0068/30/cjcp1711210
211. Xie Y, Zheng J, Lan Z. Performance evaluation of the symmetrical quasi-classical dynamics method based on Meyer-Miller mapping Hamiltonian in the treatment of site-exciton models. J Chem Phys. 2018;149:174105. https://doi.org/10.1063/1.5047002
212. Zheng J, Xie Y, Jiang S, Long Y, Ning X, Lan Z. Initial sampling in symmetrical quasiclassical dynamics based on Li-Miller mapping Hamiltonian. Phys Chem Chem Phys. 2019;21:26502–14. https://doi.org/10.1039/c9cp03975a
213. Zheng J, Peng J, Xie Y, Long Y, Ning X, Lan Z. Study of the exciton dynamics in perylene bisimide (PBI) aggregates with symmetrical quasiclassical dynamics based on the Meyer-Miller mapping Hamiltonian. Phys Chem Chem Phys. 2020;22:18192–204. https://doi.org/10.1039/d0cp00648c
214. Peng J, Xie Y, Hu D, Lan Z. Analysis of bath motion in MM-SQC dynamics via dimensionality reduction approach: principal component analysis. J Chem Phys. 2021;154:094122. https://doi.org/10.1063/5.0039743
215. Hu D, Xie Y, Peng J, Lan Z. On-the-fly symmetrical quasi-classical dynamics with Meyer−Miller mapping Hamiltonian for the treatment of nonadiabatic dynamics at conical intersections. J Chem Theory Comput. 2021;17:3267–79. https://doi.org/10.1021/acs.jctc.0c01249
216. Tao G. A multi-state trajectory method for non-adiabatic dynamics simulations. J Chem Phys. 2016;144:094108. https://doi.org/10.1063/1.4943006
217. Tao G. Coherence-controlled nonadiabatic dynamics via state-space decomposition: a consistent way to incorporate Ehrenfest and Born-Oppenheimer-like treatments of nuclear motion. J Phys Chem Lett. 2016;7:4335–9. https://doi.org/10.1021/acs.jpclett.6b01857
218. Tao G. Multi-state trajectory approach to non-adiabatic dynamics: general formalism and the active state trajectory approximation. J Chem Phys. 2017;147:044107. https://doi.org/10.1063/1.4985898
219. Schwinger J. In: Biedenharn LC, Van Dam H, eds. Quantum Theory of Angular Momentum. New York: Academic Press; 1965.
220. Sakurai JJ. Modern Quantum Mechanics. New York: Addison-Wesley; 1994.
221. Flammia ST, Liu Y-K. Direct fidelity estimation from few Pauli measurements. Phys Rev Lett. 2011;106:230501. https://doi.org/10.1103/PhysRevLett.106.230501
222. Sperling J, Walmsley IA. Quasiprobability representation of quantum coherence. Phys Rev A. 2018;97:062327. https://doi.org/10.1103/PhysRevA.97.062327
223. Bohmann M, Agudelo E, Sperling J. Probing nonclassicality with matrices of phase-space distributions. Quantum. 2020;4:16. https://doi.org/10.22331/q-2020-10-15-343
224. Bohmann M, Agudelo E. Phase-space inequalities beyond negativities. Phys Rev Lett. 2020;124:133601. https://doi.org/10.1103/PhysRevLett.124.133601
225. Lutterbach LG, Davidovich L. Method for direct measurement of the Wigner function in cavity QED and ion traps. Phys Rev Lett. 1997;78:2547–50. https://doi.org/10.1103/PhysRevLett.78.2547
226. Signoles A, Facon A, Grosso D, Dotsenko I, Haroche S, Raimond J-M, et al. Confined quantum Zeno dynamics of a watched atomic arrow. Nat Phys. 2014;10:715–9. https://doi.org/10.1038/nphys3076
227. Leiner D, Glaser SJ. Wigner process tomography: visualization of spin propagators and their spinor properties. Phys Rev A. 2018;98: 012112. https://doi.org/10.1103/PhysRevA.98.012112
228. Tian Y, Wang Z, Zhang P, Li G, Li J, Zhang T. Measurement of complete and continuous Wigner functions for discrete atomic systems. Phys Rev A. 2018;97:013840. https://doi.org/10.1103/PhysRevA.97.013840
229. Chen B, Geng J, Zhou F, Song L, Shen H, Xu N. Quantum state tomography of a single electron spin in diamond with Wigner function reconstruction. Appl Phys Lett. 2019;114:041102. https://doi.org/10.1063/1.5082878

230. Jing Y, Fadel M, Ivannikov V, Byrnes T. Split spin-squeezed Bose-Einstein condensates. New J Phys. 2019;21:093038. https://doi.org/10.1088/1367-2630/ab3fcf
231. Song C, Xu K, Li H, Zhang Y-R, Zhang X, Liu W, et al. Generation of multicomponent atomic Schrödinger cat states of up to 20 qubits. Science. 2019;365:574–7. https://doi.org/10.1126/science.aay0600
232. Eichler C, Lang C, Fink JM, Govenius J, Filipp S, Wallraff A. Observation of entanglement between itinerant microwave photons and a superconducting qubit. Phys Rev Lett. 2012;109:240501. https://doi.org/10.1103/PhysRevLett.109.240501
233. Morin O, Huang K, Liu J, Le Jeannic H, Fabre C, Laurat J. Remote creation of hybrid entanglement between particle-like and wave-like optical qubits. Nat Photon. 2014;8:570–4. https://doi.org/10.1038/nphoton.2014.137
234. Agudelo E, Sperling J, Costanzo LS, Bellini M, Zavatta A, Vogel W. Conditional hybrid nonclassicality. Phys Rev Lett. 2017;119:120403. https://doi.org/10.1103/PhysRevLett.119.120403
235. Banaszek K, Radzewicz C, Wódkiewicz K, Krasiński JS. Direct measurement of the Wigner function by photon counting. Phys Rev A. 1999;60:674–7. https://doi.org/10.1103/PhysRevA.60.674
236. Garon A, Zeier R, Glaser SJ. Visualizing operators of coupled spin systems. Phys Rev A. 2015;91:042122. https://doi.org/10.1103/PhysRevA.91.042122
237. Koczor B, Zeier R, Glaser SJ. Time evolution of coupled spin systems in a generalized Wigner representation. Ann Phys. 2019;408:1–50. https://doi.org/10.1016/j.aop.2018.11.020
238. Davies BI, Rundle RP, Dwyer VM, Samson JH, Tilma T, Everitt MJ. Visualizing spin degrees of freedom in atoms and molecules. Phys Rev A. 2019;100:042102. https://doi.org/10.1103/PhysRevA.100.042102
239. Rundle RP, Davies BI, Dwyer VM, Tilma T, Everitt MJ. Visualization of correlations in hybrid discrete-continuous variable quantum systems. J Phys Commun. 2020;4:025002. https://doi.org/10.1088/2399-6528/ab6fb6
240. Ehrenfest P. Bemerkung über die angenäherte gültigkeit der klassischen mechanik innerhalb der quantenmechanik. Z Phys. 1927;45:455–7. https://doi.org/10.1007/BF01329203
241. Li X, Tully JC, Schlegel HB, Frisch MJ. Ab initio Ehrenfest dynamics. J Chem Phys. 2005;123:084106. https://doi.org/10.1063/1.2008258
242. Tully JC. Molecular dynamics with electronic transitions. J Chem Phys. 1990;93:1061–71. https://doi.org/10.1063/1.459170
243. Wang L, Akimov A, Prezhdo OV. Recent progress in surface hopping: 2011-2015. J Phys Chem Lett. 2016;7:2100–12. https://doi.org/10.1021/acs.jpclett.6b00710
244. Peng J, Xie Y, Hu D, Du L, Lan Z. Treatment of nonadiabatic dynamics by on-the-fly trajectory surface hopping dynamics. Acta Physico-Chim Sin. 2019;35:28–48. https://doi.org/10.3866/PKU.WHXB201801042
245. Meyer KR, Hall GR. Introduction to Hamiltonian Dynamical Systems and the N-Body Problem. New York: Springer; 1992. https://doi.org/10.1007/978-1-4757-4073-8
246. Yarkony DR. Conical intersections: diabolical and often misunderstood. Acc Chem Res. 1998;31:511–8. https://doi.org/10.1021/ar970113w
247. Paterson MJ, Bearpark MJ, Robb MA, Blancafort L, Worth GA. Conical intersections: a perspective on the computation of spectroscopic Jahn-Teller parameters and the degenerate 'intersection space'. Phys Chem Chem Phys. 2005;7:2100–15. https://doi.org/10.1039/b416538a
248. Matsika S, Krause P. Nonadiabatic Events and Conical Intersections. Annu Rev Phys Chem. 2011;62:621–43. https://doi.org/10.1146/annurev-physchem-032210-103450
249. Makarov DE, Makri N. Path integrals for dissipative systems by tensor multiplication: condensed phase quantum dynamics for arbitrarily long time. Chem Phys Lett. 1994;221:482–91. https://doi.org/10.1016/0009-2614(94)00275-4
250. Makri N, Makarov DE. Tensor propagator for iterative quantum time evolution of reduced density matrices. II. Numerical methodology. J Chem Phys. 1995;102:4611–8. https://doi.org/10.1063/1.469509
251. Makri N, Makarov DE. Tensor propagator for iterative quantum time evolution of reduced density matrices. I Theory J Chem Phys. 1995;102:4600–10. https://doi.org/10.1063/1.469508
252. Topaler M, Makri N. Path integral calculation of quantum nonadiabatic rates in model condensed phase reactions. J Phys Chem. 1996;100:4430–6. https://doi.org/10.1021/jp951673k
253. Tanimura Y, Kubo R. Time evolution of a quantum system in contact with a nearly Gaussian-Markoffian noise bath. J Physical Soc Japan. 1989;58:101–14. https://doi.org/10.1143/JPSJ.58.101
254. Yan Y-A, Yang F, Liu Y, Shao J. Hierarchical approach based on stochastic decoupling to dissipative systems. Chem Phys Lett. 2004;395:216–21. https://doi.org/10.1016/j.cplett.2004.07.036
255. Xu R-X, Cui P, Li X-Q, Mo Y, Yan Y. Exact quantum master equation via the calculus on path integrals. J Chem Phys. 2005;122:041103. https://doi.org/10.1063/1.1850899
256. Shao J. Stochastic description of quantum open systems: formal solution and strong dissipation limit. Chem Phys. 2006;322:187–92. https://doi.org/10.1016/j.chemphys.2005.08.007
257. Moix JM, Cao JS. A hybrid stochastic hierarchy equations of motion approach to treat the low temperature dynamics of non-Markovian open quantum systems. J Chem Phys. 2013;139:134106. https://doi.org/10.1063/1.4822043
258. Tanimura Y. Reduced hierarchical equations of motion in real and imaginary time: correlated initial states and thermodynamic quantities. J Chem Phys. 2014;141:044114. https://doi.org/10.1063/1.4890441
259. Yan Y. Theory of open quantum systems with bath of electrons and phonons and spins: many-dissipation density matrixes approach. J Chem Phys. 2014;140:054105. https://doi.org/10.1063/1.4863379

260. Tang Z, Ouyang X, Gong Z, Wang H, Wu J. Extended hierarchy equation of motion for the spin-boson model. J Chem Phys. 2015;143:224112. https://doi.org/10.1063/1.4936924
261. Tanimura Y. Real-time and imaginary-time quantum hierarchal Fokker-Planck equations. J Chem Phys. 2015;142:144110. https://doi.org/10.1063/1.4916647
262. Meyer H-D, Manthe U, Cederbaum LS. The multi-configurational time-dependent Hartree approach. Chem Phys Lett. 1990;165:73–8. https://doi.org/10.1016/0009-2614(90)87014-i
263. Thoss M, Wang H, Miller WH. Self-consistent hybrid approach for complex systems: application to the spin-boson model with Debye spectral density. J Chem Phys. 2001;115:2991–3005. https://doi.org/10.1063/1.1385562
264. Wang H, Thoss M, Miller WH. Systematic convergence in the dynamical hybrid approach for complex systems: a numerically exact methodology. J Chem Phys. 2001;115:2979–90. https://doi.org/10.1063/1.1385561
265. Wang H, Thoss M. Multilayer formulation of the multiconfiguration time-dependent Hartree theory. J Chem Phys. 2003;119:1289–99. https://doi.org/10.1063/1.1580111
266. Wang H, Thoss M. From coherent motion to localization: dynamics of the spin-boson model at zero temperature. New J Phys. 2008;10:115005. https://doi.org/10.1088/1367-2630/10/11/115005
267. Worth GA, Meyer H-D, Köppel H, Cederbaum LS, Burghardt I. Using the MCTDH wavepacket propagation method to describe multimode non-adiabatic dynamics. Int Rev Phys Chem. 2008;27:569–606. https://doi.org/10.1080/01442350802137656
268. Wang H, Thoss M. From coherent motion to localization: II. Dynamics of the spin-boson model with sub-Ohmic spectral density at zero temperature. Chem Phys. 2010;370:78–86. https://doi.org/10.1016/j.chemphys.2010.02.027
269. Craig IR, Thoss M, Wang H. Proton transfer reactions in model condensed-phase environments: accurate quantum dynamics using the multilayer multiconfiguration time-dependent Hartree approach. J Chem Phys. 2007;127:144503. https://doi.org/10.1063/1.2772265
270. Wang H. Iterative calculation of energy eigenstates employing the multilayer multiconfiguration time-dependent Hartree theory. J Phys Chem A. 2014;118:9253–61. https://doi.org/10.1021/jp503351t
271. Purcell EM. Spontaneous Emission Probabilities at Radio Frequencies. In: Burstein E, Weisbuch C, editors. Confined Electrons and Photons: New Physics and Applications. Boston, MA: Springer US; 1995. https://doi.org/10.1007/978-1-4615-1963-8_40
272. Krasnok AE, Slobozhanyuk AP, Simovski CR, Tretyakov SA, Poddubny AN, Miroshnichenko AE, et al. An antenna model for the Purcell effect. Sci Rep. 2015;5:12956. https://doi.org/10.1038/srep12956
273. Rybin MV, Mingaleev SF, Limonov MF, Kivshar YS. Purcell effect and Lamb shift as interference phenomena. Sci Rep. 2016;6:20599. https://doi.org/10.1038/srep20599
274. Holsteen AL, Raza S, Fan P, Kik PG, Brongersma ML. Purcell effect for active tuning of light scattering from semiconductor optical antennas. Science. 2017;358:1407–10. https://doi.org/10.1126/science.aao5371
275. Alagappan G, Krivitsky LA, Png CE. Diamond in a nanopocket: a new route to a strong Purcell effect. ACS Omega. 2018;3:4733–42. https://doi.org/10.1021/acsomega.8b00139
276. Gallego J, Alt W, Macha T, Martinez-Dorantes M, Pandey D, Meschede D. Strong Purcell effect on a neutral atom trapped in an open fiber cavity. Phys Rev Lett. 2018;121:173603. https://doi.org/10.1103/PhysRevLett.121.173603
277. Ren T, Dong Y, Xu S, Gong X. Strong Purcell effect in deep subwavelength coaxial cavity with GeSn active medium. Opt Lett. 2021;46:3889–92. https://doi.org/10.1364/OL.432164
278. Carmichael HJ, Brecha RJ, Raizen MG, Kimble HJ, Rice PR. Subnatural linewidth averaging for coupled atomic and cavity-mode oscillators. Phys Rev A. 1989;40:5516–9. https://doi.org/10.1103/physreva.40.5516
279. Zhu Y, Gauthier DJ, Morin SE, Wu Q, Carmichael HJ, Mossberg TW. Vacuum Rabi splitting as a feature of linear-dispersion theory: analysis and experimental observations. Phys Rev Lett. 1990;64:2499–502. https://doi.org/10.1103/PhysRevLett.64.2499
280. Field JE. Vacuum-Rabi-splitting-induced transparency. Phys Rev A. 1993;47:5064–7. https://doi.org/10.1103/physreva.47.5064
281. Abram I, Oudar JL. Spontaneous emission in planar semiconductor microcavities displaying vacuum Rabi splitting. Phys Rev A. 1995;51:4116–22. https://doi.org/10.1103/physreva.51.4116
282. Li K, Wang W, Chen Z, Gao N, Yang W, Li W, et al. Vacuum Rabi splitting of exciton-polariton emission in an AlN film. Sci Rep. 2013;3:3551. https://doi.org/10.1038/srep03551
283. Toida H, Nakajima T, Komiyama S. Vacuum Rabi splitting in a semiconductor circuit QED system. Phys Rev Lett. 2013;110:066802. https://doi.org/10.1103/PhysRevLett.110.066802
284. Guerin W, Santo T, Weiss P, Cipris A, Schachenmayer J, Kaiser R, et al. Collective multimode vacuum Rabi splitting. Phys Rev Lett. 2019;123:243401. https://doi.org/10.1103/PhysRevLett.123.243401
285. Yan Y, Ergogo TT, Lü Z, Chen L, Luo J, Zhao Y. Lamb shift and the vacuum Rabi splitting in a strongly dissipative environment. J Phys Chem Lett. 2021;12:9919–25. https://doi.org/10.1021/acs.jpclett.1c02791
286. Meystre P, Sargent M. Elements of Quantum Optics. Berlin Heidelberg: Springer; 2007. https://doi.org/10.1007/978-3-540-74211-1
287. Hoffmann NM, Schäfer C, Rubio A, Kelly A, Appel H. Capturing vacuum fluctuations and photon correlations in cavity quantum electrodynamics with multitrajectory Ehrenfest dynamics. Phys Rev A. 2019;99:063819. https://doi.org/10.1103/PhysRevA.99.063819
288. Hoffmann NM, Schäfer C, Säkkinen N, Rubio A, Appel H, Kelly A. Benchmarking semiclassical and perturbative methods for real-time simulations of cavity-bound emission and interference. J Chem Phys. 2019;151:244113. https://doi.org/10.1063/1.5128076
289. Li TE, Chen HT, Nitzan A, Subotnik JE. Quasiclassical modeling of cavity quantum electrodynamics. Phys Rev A. 2020;101:033831. https://doi.org/10.1103/PhysRevA.101.033831
290. Levine BG, Ko C, Quenneville J, Martínez TJ. Conical intersections and double excitations in time-dependent density functional theory. Mol Phys. 2006;104:1039–51. https://doi.org/10.1080/00268970500417762

291. Halcrow MA. Jahn-Teller distortions in transition metal compounds, and their importance in functional molecular and inorganic materials. Chem Soc Rev. 2013;42:1784–95. https://doi.org/10.1039/c2cs35253b
292. Bersuker IB. The Jahn-Teller and pseudo-Jahn-Teller effects: a unique and only source of spontaneous symmetry breaking in atomic matter. Symmetry. 2021;13:1577. https://doi.org/10.3390/sym13091577
293. Qin A, Lam JWY, Tang BZ. Luminogenic polymers with aggregation-induced emission characteristics. Prog Polym Sci. 2012;37:182–209. https://doi.org/10.1016/j.progpolymsci.2011.08.002
294. Schneider R, Domcke W. S1-S2 Conical intersection and ultrafast S2->S1 Internal conversion in pyrazine. Chem Phys Lett. 1988;150:235–42. https://doi.org/10.1016/0009-2614(88)80034-4
295. Hacker B, Welte S, Daiss S, Shaukat A, Ritter S, Li L, et al. Deterministic creation of entangled atom-light Schrodinger-cat states. Nat Photon. 2019;13:110–5. https://doi.org/10.1038/s41566-018-0339-5
296. Vlastakis B, Petrenko A, Ofek N, Sun L, Leghtas Z, Sliwa K, et al. Characterizing entanglement of an artificial atom and a cavity cat state with Bell's inequality. Nat Commun. 2015;6:8970. https://doi.org/10.1038/ncomms9970
297. Isserlis L. On a formula for the product-moment coefficient of any order of a normal frequency distribution in any number of variables. Biometrika. 1918;12:134–9. https://doi.org/10.1093/biomet/12.1-2.134
298. Wang MC, Uhlenbeck GE. On the theory of the Brownian motion II. Rev Mod Phys. 1945;17:323–42. https://doi.org/10.1103/revmodphys.17.323
299. Fano U. Geometrical characterization of nuclear states and the theory of angular correlations. Phys Rev. 1953;90:577–9. https://doi.org/10.1103/PhysRev.90.577
300. Tilma T, Sudarshan ECG. Generalized Euler angle parameterization for U(N) with applications to SU(N) coset volume measures. J Geometry Phys. 2004;52:263–83. https://doi.org/10.1016/j.geomphys.2004.03.003
301. Tilma T, Sudarshan ECG. Generalized Euler angle parametrization for SU(N). J Phys A Math Gen. 2002;35:10467–501. https://doi.org/10.1088/0305-4470/35/48/316
302. Klimov AB. Exact evolution equations for SU(2) quasidistribution functions. J Math Phys. 2002;43:2202–13. https://doi.org/10.1063/1.1463711
303. Bóna P. Classical Systems in Quantum Mechanics. Cham: Springer; 2020. https://doi.org/10.1007/978-3-030-45070-0_3
304. Makri N. Small matrix disentanglement of the path integral: overcoming the exponential tensor scaling with memory length. J Chem Phys. 2020;152:041104. https://doi.org/10.1063/1.5139473
305. Makri N. Small matrix path integral for system-bath dynamics. J Chem Theory Comput. 2020;16:4038–49. https://doi.org/10.1021/acs.jctc.0c00987
306. Makri N. The linear response approximation and its lowest order corrections: an influence functional approach. J Phys Chem B. 1999;103:2823–9. https://doi.org/10.1021/jp9847540

## SUPPORTING INFORMATION

Additional supporting information may be found in the online version of the article at the publisher's website.

**How to cite this article:** He X, Wu B, Shang Y, Li B, Cheng X, Liu J. New phase space formulations and quantum dynamics approaches. WIREs Comput Mol Sci. 2022. e1619. https://doi.org/10.1002/wcms.1619